ATTENUATING INFLAMMATION BY MODULATING MICRORNA-155 EXPRESSION IN MACROPHAGES USING LIPID NANOPARTICLES AND EXTRACELLULAR VESICLES

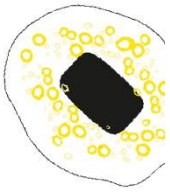

Miranda Türkal (S2538008)

Biomedical Engineering (Bioengineering Technologies)

MASTER'S THESIS

Faculty of Science and Technology (TNW)

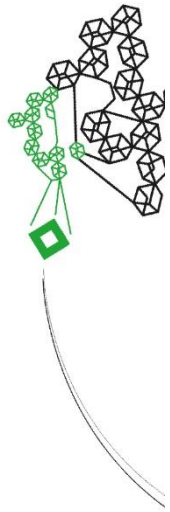

COMMITTEE

c Ruchi Bansal

Dr. Pieter Vader

MSc. Eline Geervliet

TLR Translational Liver Research

MCBP

UNIVERSITY OF TWENTE.

Preface

First of all, I would like to thank my supervisor, Dr. Ruchi Bansal, for giving me the chance to complete my thesis in her group Translational Liver Research (TRL). I am grateful for all the opportunities she gave me; it was a privilege to have her support throughout my research. Secondly, I would like to extend my thanks to my daily supervisor Eline Geervliet who was always there whenever I needed her and always patient with my questions. Being a member of the TRL research group was a priceless experience for me, and personally, it prepared me to be ready for the next challenges. Lastly, I also want to thank my other committee member, Dr. Pieter Vader, for being a member of my committee.

I would not be able to achieve this without the support of my family and my friends. Hence, I also want to express my gratitude to my lovely family and friends.

Table of Contents

List of Abbreviations

Abbreviation	Full form
3T3	mouse fibroblast cells
AB	Alamar blue
Abs	antibodies
ALT	alanine transferase
AML-12	mouse hepatocytes cells
AMSCs	adipose MSCs
antimiRs	Anti-microRNAs
ApoE	apolipoprotein E
ARG-1	arginase 1
ASO	antisense oligonucleotides
AST	aspartate aminotransferase
CDAA	choline-deficient-amino-acid-defined
CTCL	cutaneous T-cell lymphoma
DAMPs	damage-associated molecular patterns
DC	dendritic cells
DiD	lipophilic carbocyanine DiD fluorescent dye
DLS	dynamic light scattering
DMEM	Dulbecco's modified Eagle's medium
DSPC	phosphatidylcholine
EE	encapsulation efficiency
EGF	epidermal growth factor
EPR	enhanced permeability and retention effect
Evs	extracellular vesicles
Exo-AMSCs	adipose MSCs-derived exosomes
FACS	Fluorescence-Activated Cell Sorting
FBS	fetal bovine serum
FFA	free fatty acid
FFR	flow rate ratio
H5V	mouse endothelial cells
HBSS	Hanks' Balanced Salt Solution
HCC	hepatocellular carcinoma
HCV	Hepatitis C virus
HSC	hepatic stellate cell
IFN-γ	interferon gamma
IL-1β	interleukin 1-beta
KC	Kupffer cells
KO	knockout
Lac-GLN	lactosylated gramicidin containing LNPs
LDLr	low-density lipoprotein receptor
LE	loading efficiency
LNA	locked nucleic acid
LNPs	lipid nanoparticles
LPS	lipopolysaccharide

LSECs	liver sinusoidal endothelial cells
LV	Lentiviral
mAB	monoclonal antibody
MC3	DLin-MC3-DMA
MCD	methionine/choline deficient
miRNAs, miRs	microRNAs
MRC-1	mannose receptor C-type 1
MRG-106	Cobomarsen
MSCs	mesenchymal stem cells
MWCO	molecular weight cut-off
NAFLD	nonalcoholic fatty liver disease
NASH	non-alcoholic steatohepatitis
NF-κB	nuclear factor kappa-light-chain-enhancer of activated B cells
NLRP3	NOD-, LRR- and pyrin domain-containing protein 3
NTA	nanoparticle tracking analysis
OA	oleic acid
PA	palmitic acid
PAMPs	pathogen-associated molecular patterns
PBS	phosphate buffered saline
PEG-DMG	polyethylene glycol-dimyristolglycerol
PDGF	platelet-derived growth factor
PDI	polydispersity index
PEG	polyethylene glycol
pre-miRNAs	precursor-miRNAs
pri-miRNAs	primary miRNA
qPCR	quantitative polymerase chain reaction
RAW 264.7	mouse macrophages cells
RES	reticuloendothelial system
RISC	RNA-induced silencing complex
RNA	ribonucleic acid
ROS	reactive oxygen species
RPMI1640	Roswell Park medium institute1640
SD	standard deviation
STAT3	signal transducer and activator of transcription 3
TGF-β	transforming growth factor β
TLR4	toll-like receptor 4
TMB	3,3’,5,5’-tetramethylbenzidine
TNFα	tumor necrosis factor alpha
UTRs	untranslated regions

Abstract

Nonalcoholic fatty liver disease (NAFLD) is becoming a major health-related burden due to its growing prevalence worldwide. NAFLD comprises a wide range of liver diseases, including nonalcoholic steatohepatitis (NASH). NASH is characterized by liver cell damage, inflammation, hepatocellular ballooning, and an alternating range of fibrosis. Despite the wide distribution of NASH in populations, there is still a lack of treatment. Changes in the expression of microRNAs (miRNAs) are associated with different liver diseases, and an altered hepatic miRNA profile has been described in NASH. MiRNAs, small non-coding RNAs that can regulate post-transcriptional gene expression by binding target mRNAs. MiR-155 is considered the main inflammation modulator in the liver and its overexpression was observed in inflammatory macrophages upon LPS stimulation. The main objective of this project is to establish an antimiR-155 delivery platform to the liver macrophages to attenuate liver inflammation by reducing miR-155 and pro-inflammatory cytokine expressions. Lipid nanoparticles (LNPs) are one of the most advance non-viral delivery platforms for negatively charged nucleic acids. In this study, for the first time, we delivered antimiR-155 to inflammatory macrophages by using MC3 lipid-containing LNPs to alleviate the inflammatory response. We found reduced expression of TNFα and IL-6 along with miR-155 when 10mM antimiR-155 encapsulated LNPs were delivered to M1 macrophages. LNPs proved to be as efficient as commercially available transfection reagent HiPerFect while showing better tolerability in macrophages. As an alternative to LNPs, we used extracellular vesicles (EVs). Mesenchymal stem cells (MSCs)-derived exosomes show an inherent capacity to mitigate inflammation, and they are natural RNA carriers. For this project, for the first time, we used EVs derived from AMSCs transfected with antimiR-155. Even though pro-inflammatory cytokine TNFα expression did not change, we observed reduced IL-1β expression following increased anti-inflammatory markers.

1. Introduction

1.1. Nonalcoholic Steatohepatitis (NASH)

Nonalcoholic fatty liver disease (NAFLD) is becoming a major health-related burden due to its growing prevalence worldwide. Accumulation of free fatty acids and triglyceride in the liver causes NAFLD in the absence of alcohol consumption. Obesity, metabolic syndrome, and type 2 diabetes contribute to the disease formation [1]. The incidence of NAFLD is approximately 29.8% of the world population, making it the most common liver disease worldwide [2,3] From 1991 to 2019, the prevalence of NAFLD increased by 15.4% and the trend in Europe showed a 1.1% increase every year [3]. Despite the increasing numbers, no adequate therapy is available yet. To identify possible therapies, we first must investigate the disease progression/pathophysiology of NAFLD.

NAFLD comprises a wide range of liver diseases, including simple fatty liver (NAFL) and a more severe form, nonalcoholic steatohepatitis (NASH) [4]. Besides triglyceride accumulation, NASH is characterized by liver cell damage, inflammation, hepatocellular ballooning, and an alternating range of fibrosis, whereas there is no or slight inflammation in NAFL (**Figure 1**) [5,6]. Subset of all NAFLD patients develop NASH and individuals with NASH ultimately develop towards cirrhosis and/or HCC [1]. Even though cirrhosis only develops roughly 4% of people with NAFLD, more than 20% of NASH patients will eventually develop cirrhosis [7]. The standardized incidence ratio of HCC in individuals with NAFLD/NASH was 4.4% in a 16-year follow-up study. Worldwide, the prevalence of HCC linked to NAFLD/NASH is consistently rising; nevertheless, studies reveal varying prevalence rates in Western nations that range between 4% and 22% [8].

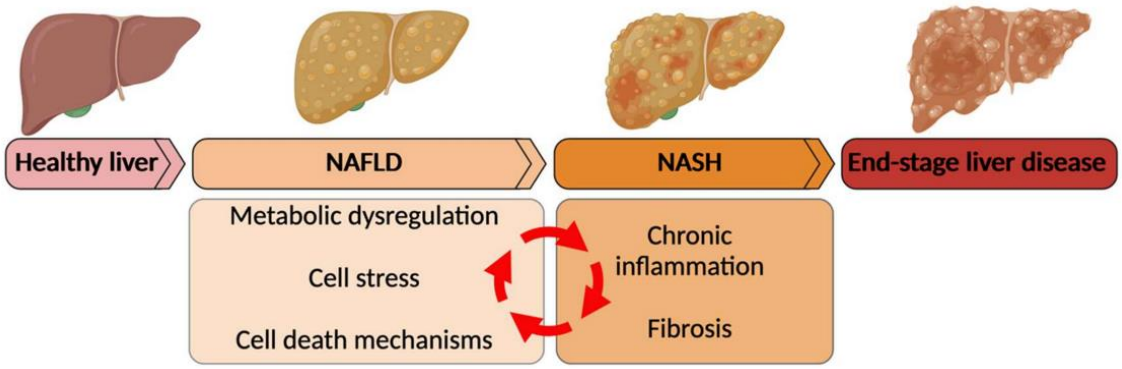

Figure 1: The spectrum of nonalcoholic fatty liver disease [9].

The pathophysiology of NASH has been considered a “multi-hit” scenario (shown in **Figure 2**). Adipose tissue dysfunction, gut-released bacterial products, genetic factors, and high-fat diet contributes to the progression of NASH [6]. In an obese state, metabolic syndrome, or unhealthy diet, a large influx of free fatty acids (FFAs) to the liver causes excessive production of reactive oxygen species (ROS) and can lead to mitochondrial dysfunction. When a cell is unable to endure mitochondrial stress, apoptotic pathways are initiated, resulting in hepatocellular damage [6,10]. Besides, in NASH, Kupffer cells (KC) and recruited macrophages are activated through various cytokines and bacterial products such as LPS and become pro-inflammatory M1 phenotype. Pattern-recognition receptor such as TLR4 is essential for the recognition of LPS by macrophages. Moreover, activation of NLPR3 inflammasome, an

intracellular multiprotein complex involved in the production of interleukin 1-beta (IL-1β), further contributes to inflammation [11]. During NASH progression, different pro-inflammatory cytokines are released. Ineffective removal of the inflammatory chemicals causes a protracted inflammation that eventually leads to fibrosis. TNFα, IL-6, and IL-1β are the main pro-inflammatory cytokines released from M1 macrophages, and levels of those found upregulated in NASH patients [12,13]. Activated M1 macrophages recruit hepatic stellate cells (HSCs), the resident fibroblastic cells, that stimulate fibrosis through the secretion of CCL2 [14]. Furthermore, gut-released bacterial products enter the liver and activate TLR4 and NLRP3 inflammasome, thus inducing the production of inflammatory cytokines such as, TNFα, and IL-6 through activated immune cells [6,15].

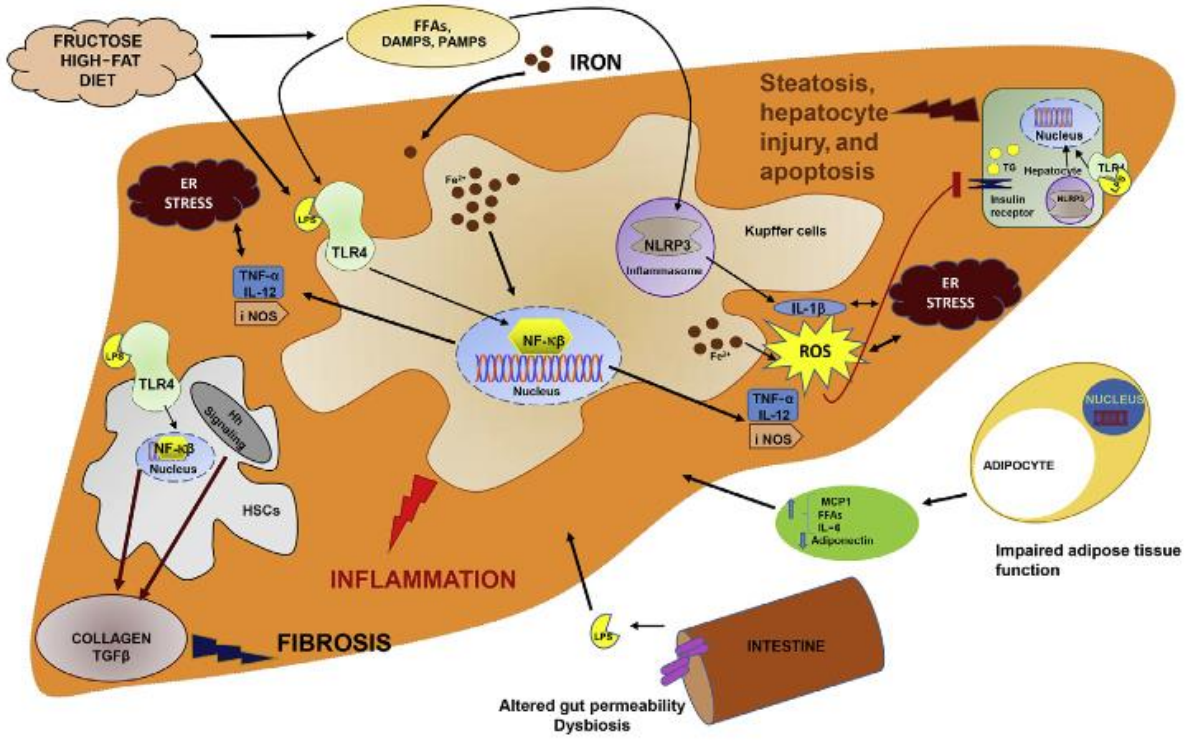

Figure 2: Multi-hit mechanisms underlying NASH progression. Adapted from Manne et al. [6]

Despite the wide distribution of NASH in populations, there is still a lack of treatment and no approved medicines. Dietary recommendations and lifestyle changes seemed to be effective but hard to maintain [16]. Even though some diabetes drugs (pioglitazone) and antioxidant drugs (vitamin E) are used to treat NASH, they show low efficiency [17]. On the other hand, immunosuppressive drugs might be used as a treatment strategy; however, long-term administration increases the risk of infectious diseases because of the sustained repression of immunity [18]. Thus, efficient alternative therapies that could overcome adverse immune responses without causing life-threatening immunosuppression are urgently necessary. Recently, changes in the expression of miRNAs are associated with different liver diseases, and an altered hepatic miRNA profile has been described in NASH. Among the roles of miRNAs, hepatic metabolic functions, adipocyte differentiation, and the control of the immune response, which are associated with NASH, have directed researchers to seek the interaction between miRNAs and NASH [19].

1.2. MicroRNA (miRNA) Biogenesis

MicroRNAs (miRNAs), small non-coding RNAs with a length of 19 to 25 nucleotides, can regulate post-transcriptional gene expression by binding to 3'-untranslated regions (UTRs) of target mRNAs [20]. MiRNAs are transcribed by RNA polymerase II, which generates the long primary transcripts characterized by hairpin structures (primary-miRNAs, pri-miRNAs) where miRNA sequences are embedded (**Figure 3**). Then, pri-miRNAs bind to the RNase III protein Drosha, which cuts the 3' and 5' strands of pri-miRNAs and generates precursor-miRNAs (pre-miRNAs). Subsequently, pre-miRNAs are exported from the nucleus into the cytosol, where Dicer cleaves them to yield a double-stranded RNA duplex made up of the mature miRNA guide strand and the complementary passenger strand. The passenger strand is usually subject to degradation, but some studies suggest that it also represents a functional strand and plays biological roles [21]. The mature miRNA guide strand contains a specific heptameric nucleotide sequence between nucleotides 2 and 8 of miRNAs called 'seed sequence', which establishes the target specificity. In the last step, the mature single-stranded miRNA is incorporated into the RNA-induced silencing complex (RISC), leading to its binding to the complementary sequences in the 3'-untranslated regions (UTRs) of target mRNAs and resulting in mRNA translational inhibition or degradation [22].

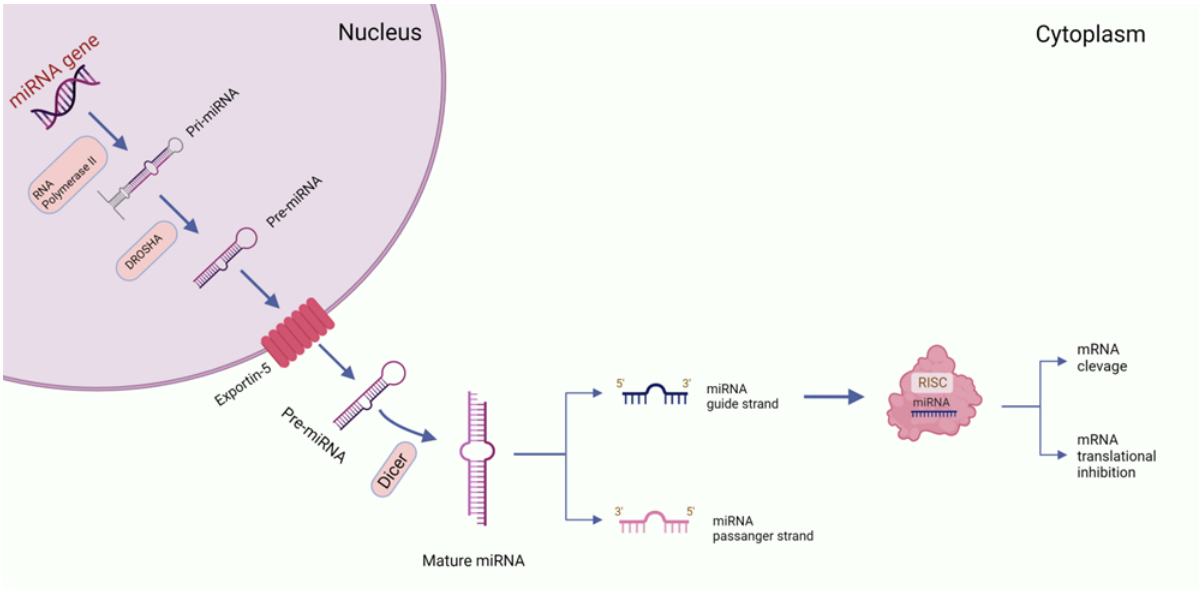

Figure 3: Biogenesis of miRNA. From the miRNA gene, RNA polymerase transcribes pri-miRNA that is cleaved by DROSHA in the nucleus. Formed pre-miR is transported to the cytoplasm through exportin-5. In the cytoplasm, Dicer cleaves pre-miR to yield mature miRNA. The passenger strand of the mature miRNA is subjected to degradation, and the guide strand is loaded into the RISC complex. Depending on the seed region of the miRNA strand, its mRNA target either gets cleaved or repressed. Created with BioRender.com

1.3. Roles of MiRNAs in Liver Inflammation

Human miRNAs are responsible for a wide range of pathological and physiological processes in the liver, such as lipid and glucose metabolism, apoptosis, necrosis, cell cycle, proliferation and inflammation [23]. Considering the key roles of miRNAs in liver diseases, the regulation of the miRNA expression is under tight and dynamic control by many regulatory factors. However, the expression can be dysregulated by different factors, including alcohol consumption, drugs and diet [24–26]. As a result of this dysregulation, miRNAs are associated with diverse pathologies in the liver such as, fibrosis, NASH, and hepatocellular carcinoma (HCC) [19,23,24,27].

In addition to the metabolic disruption, inflammation is also a major factor in NASH development and inflammation determines the long-term prognosis of NASH [28,29]. Various factors contribute to liver inflammation, including viral and bacterial infections, toxins and antigens. MiRNAs are one of the key regulators of innate and adaptive immune response by targeting various signaling molecules [30,31]. Plenty of different microRNA has been implied in the regulation of inflammatory response in NASH including, miR146a [32,33], miR-122 [34], miR-32 [35], and miR-155 [30,31]. MiR-155 is considered the main inflammation modulator in the liver and is associated with both innate and adaptive immunity by mediating the activity of macrophages and monocytes, T and B cells, and also dendritic cells [36].

1.4. MiR-155 Regulates Inflammation

MiR-155 is a multifunctional miRNA associated with common human diseases such as cancers, viral and immune-related diseases. Many studies identified different targets of miR-155 to elucidate the miR-155 and its role in different diseases [37]. Deregulation of miR-155 was correlated with enhanced risk of breast cancer while upregulation of miR-155 was related to poor survival of lung cancer patients [38]. Wang et al. demonstrated that increased miR-155 reduced the production of CCAAT/enhancer binding protein beta (C/EBPβ), which in turn facilitated the proliferation of HCC cells [39]. Moreover, in a study of 45 human HCC tissue examined, most malignant HCC tissues showed overexpressed (from 1.5-fold to 6-fold) miR-155 levels (in **Figure 4**). It was found that overexpressed miR-155 increased the HCC proliferation and tumorigenesis [40]. Another group highlighted the oncogenic miR-155 contribution to linking liver inflammation to cancer. It was shown that miR-155 expression was upregulated by HCV infection in a nuclear factor kappa B (NF-κB)-dependent manner, which promoted carcinogenesis by activating WNT signaling [41]. Moreover, miRNA expression array from patients showed that miR-155 was significantly upregulated in NASH and HCV induced cirrhosis (in **Figure 5**) [42].

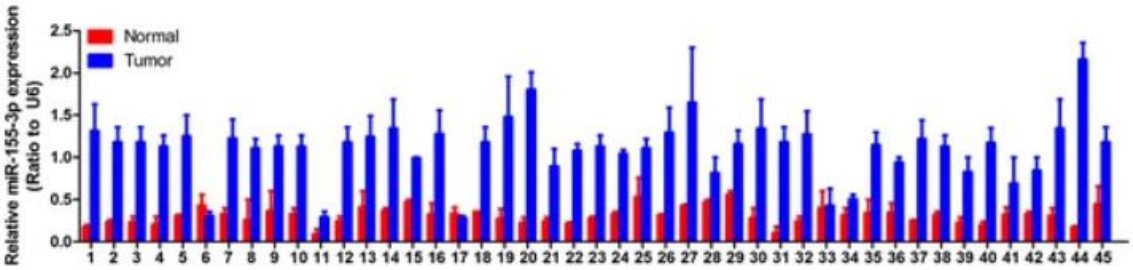

Figure 4: The expression of miR-155 is elevated in Hepatocellular carcinoma tissues. miR-155-3p expression in Hepatocellular carcinoma in comparison to normal tissues was measured by qRT-PCR [40].

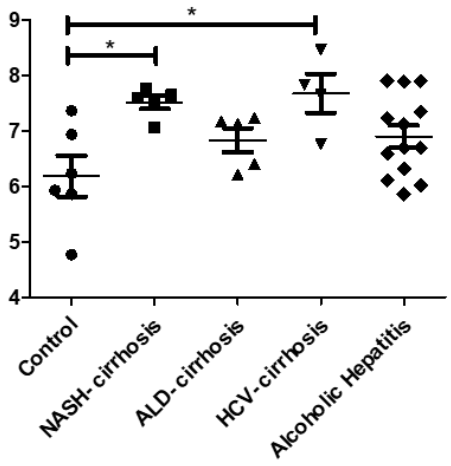

Figure 5: miRNA expression array results of liver diseases patients. Adapted from Blaya et al. [42].

In the liver, hepatocytes, endothelial cells, and inflammatory cells such as natural killer cells, macrophages, and monocytes express miR-155. It is known that miR-155 contributes to the correction of the development of immune cells, mediating immune response, and regulating oncogenic pathways [37,43,44]. miR-155 is a master of inflammation which regulates pro-inflammatory activation of macrophages and dendritic cells (in **Figure 6**). TNFα, pathogen-associated molecular patterns and damage-associated molecular patterns (PAMPs/DAMPs) are among the inflammatory mediators which induce miR-155 expression. MiR-155 targets SHIP-1, SOCS-1, and BCL6 to promote the production of pro-inflammatory cytokines also represses anti-inflammatory and repair macrophage phenotypes by targeting IL-13Rα, LXRα, and the TGFβ-signaling molecule SMAD2 [45]. Upon lipopolysaccharide (LPS) and/or interferon-gamma (IFN-γ) activation of the macrophages, the expression level of miR-155 is enhanced in a concentration-dependent manner (in **Figure 7**) [46–49].

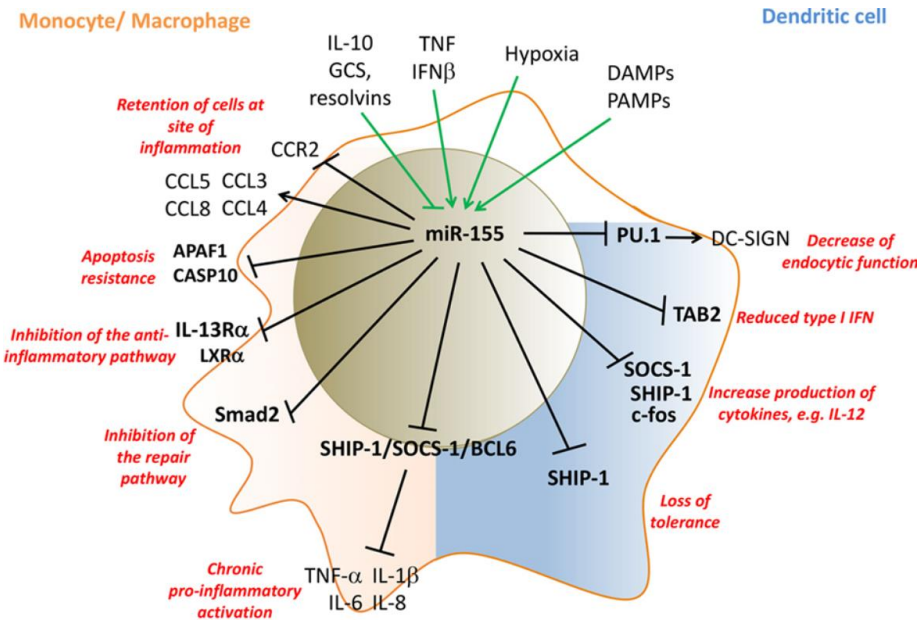

Figure 6: MiR-155 controls the pro-inflammatory activation of dendritic cells (DCs) (blue) and monocytes/macrophages (pink). Adapted from Alivernini et al. [45].

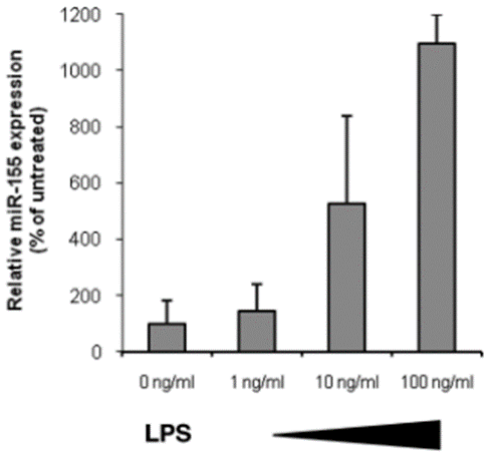

Figure 7: LPS-mediated induction of miR-155 in cultured mouse Raw264.7 macrophages [49].

In choline-deficient-amino-acid-defined (CDAA) and high-fat diet models of steatohepatitis, overexpression of miR-155 has been observed [39,50]. Furthermore, Csak et al. [51] showed methionine-choline-deficient (MCD) fed mice developed steatohepatitis along with enhanced miR-155 expression in total liver, hepatocytes and Kupffer cells (in **Figure 8**).

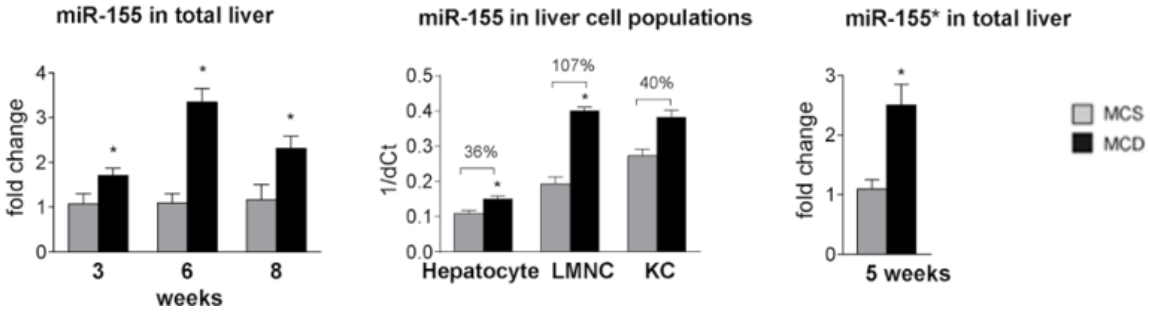

Figure 8: miR-155 expression in parenchymal and non-parenchymal cells after induction of steatohepatitis. C57Bl/6 mice were fed with methionine-choline deficient (MCD) or supplemented (MCS) control diet for 3, 6 and 8 weeks [51].

The elevated miR-155 expression exerts a positive regulation on the release of TNFα [46]. TNFα has a central role in the pathogenesis of NASH. Therefore, targeting TNFα secretion could be a promising approach for treating liver inflammation. It was shown that miR-155 participates in a positive feedback mechanism with TNFα, where enhanced level of miR-155 increases the level of TNFα [52]. Moreover, a linear correlation between miR-155 and TNFα was found in LPS-treated RAW 264.7 cells (in **Figure 9**). Inhibition of miR-155 resulted in lower levels of TNFα in macrophages [53].

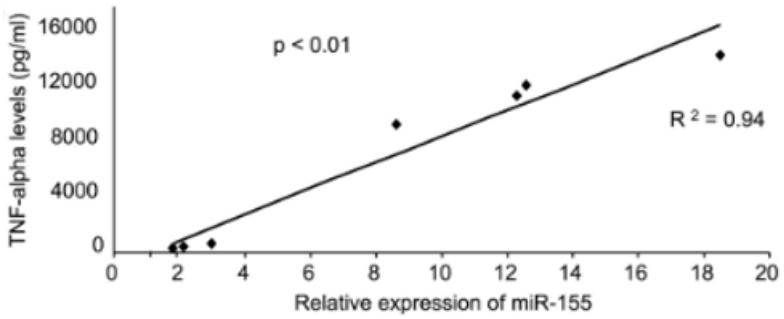

Figure 9: **TNFα production is increased in RAW 264.7 macrophages after LPS and/or alcohol treatment and correlates with miR-155 expression**. [53]

Inflammatory macrophages secrete other cytokines such as IL-1β, IL-6 and IL-12. [54] Jablonski et al. associated upregulated expression of IL-1β, IL-6, TNF-α, NO and IL-12 with miR-155 dependent pathways. In miR-155 KO mice, macrophages failed to express M1 markers, including TNFα and IL-1β. [48] Other studies revealed that miR-155 is responsible for the post-translational regulation of TNFα in macrophages [52], and miR155 expression increases through NF-κB-mediated mechanism. [32] In addition, comparative transcriptional profiling demonstrated that miR-155 regulates approximately 650 genes related to inflammatory phenotype of M1 macrophages. [48] Considering the inflammation stimulatory role of miR-155 in macrophages, targeting miR-155 for treating liver inflammation could be a promising approach for NASH treatment.

1.5. MiRNA Therapeutics and Nanocarriers

Due to the roles of miRNAs in development, proliferation, and homeostasis, misregulation of miRNAs is critical in disease development and progression. In different diseases, miRNA levels can be under/overexpressed; thus, a miRNA therapeutic can function to either induce the expression or reduce it [55]. In general, to be able to increase the level of miRNA, which had downregulated, synthetic miRNA mimics are used. These mimics share the same sequence as the endogenous miRNA, and they can boost mRNA degradation by re-establishing the function of miRNA. Conversely, if the overexpression of miRNA causes the malfunction, miRNA silencing approaches can be taken, such as miRNA antisense oligonucleotides (ASOs) and anti-microRNAs (antimiRs) (in **Figure 10**) [56].

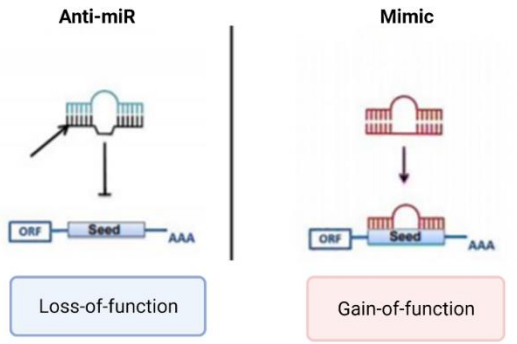

Figure 10: **Different approaches to targeting miRNA activity.** Created with BioRender.com

Despite the rapidly increasing miRNA therapeutic area, *in vivo* delivery of miRNA therapeutics remains challenging due to the low membrane permeability, rapid clearance from circulation, and degradation of miRNAs. Therefore, introducing a delivery vehicle and chemical modifications of oligonucleotides are necessary [57]. Identifying the ideal therapeutic miRNA chemistry is crucial to targeting specific miRNAs efficiently. Therefore, oligonucleotides are modified to increase stability and, consequently, efficacy. Chemical modifications can be beneficial to increase the protection from nuclease degradation and plasma clearance or to induce tissue uptake [58]. Modifications can include 2'-O–Me, 2'-F, 2'-O- (2-methoxyethyl) (2'MOE), cholesterol modification, locked nucleic acid (LNA) modification, and phosphorothioate [59–62].

Regardless of the vast potential and versatility of miRNA therapeutics, no miRNA-based therapeutics have entered the market yet. However, there are a lot of biotech companies that are intensely working on miRNA technologies. For instance, Miraversen is a phosphorothioate-modified LNA antagomir that aims to attenuate Hepatitis C virus (HCV) by targeting liver-specific miR-122. The first miRNA therapeutic that entered the clinical trial is MRX34, developed by Mirna Therapeutics Inc. (Synlogic). MRX34 was delivered as a double-stranded RNA encapsulated in a liposome nanoparticle for the treatment of renal cell carcinoma and hepatocellular carcinoma. Unfortunately, the clinical trial of MRX34 was terminated due to the immune-related severe side effects. Even though microRNA therapeutics have a huge potential for treating complex diseases due to their multiple targeting characteristics, finding the correct carrier is crucial to increasing the delivery efficiency, reducing the dosage, and preventing the off-targets [55,63]. Up to now, there is only one microRNA-based therapeutics, RG-125, enrolled in clinical trials for NASH treatment. RG-125 is a miR-103/107 antimiR that function as an effective immune sensitizer for the treatment of NASH patients with type 2 diabetes. However, AstraZeneca halted the development of RG-125 in 2017 [64]. On the other hand, the LNA-modified oligonucleotide inhibitor of miR-155, MRG-106 (Cobomarsen), is currently in clinical trial Phase 1 for the treatment of cutaneous T-cell lymphoma (CTCL). Due to the accessibility of cutaneous lesions, Cobomarsen does not need any delivery vehicle. Promising results of Cobomarsen emphasize the potential of miR-155 therapeutics [65].

1.5.1. Lipid Nanoparticles (LNPs)

Lipid nanoparticles (LNPs) are one of the most advance non-viral delivery platforms for negatively charged nucleic acids. LNPs used for oligonucleotide delivery generally consist of helper lipid (phospholipid), PEGylating lipid, cholesterol and ionizable lipid (shown in **Figure 11**, left panel) [66,67]. Phospholipids yield bilayer phase formation due to their cylindrical geometry. Lipid bilayers encapsulate oligonucleotides in their aqueous core and between bilayers (**Figure 11**, right panel). The incorporation of PEGylating lipid is the determined of the size of LNPs while increases the circulating time by increasing the colloidal stability and the resistance to serum proteins. Moreover, cholesterol further stabilizes the nanoparticle by filling the gaps between lipids and improving membrane fluidity. Lastly, ionizable lipid DLin-MC3-DMA is negatively charge at pH4 which enables the loading of nucleic acids and neutral at pH7.4. Therefore, when LNPs delivered to the cells, acidic pH in endosomes causes conformational change in LNP structure and stimulate endosomal escape [66,68]. LNPs have shown promise as delivery vehicles for enhancing the therapeutic efficacy of RNAs by protecting degradation

of miRNAs from serum nucleases, increasing circulation time, improving tumor uptake and facilitate the internalization of the oligonucleotide [68].

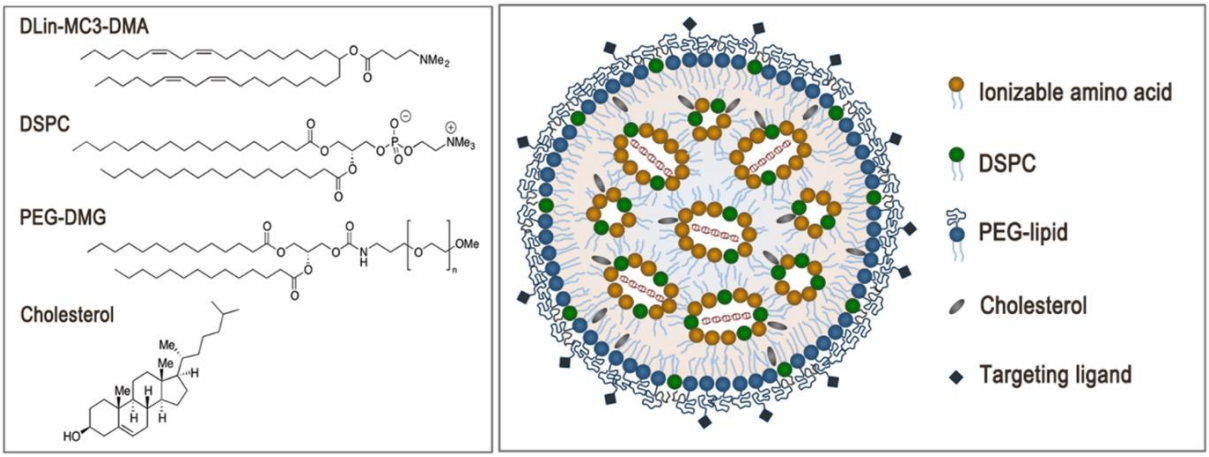

Figure 11: Structure of lipids in LNP formulation (on the left panel) and LNP (on the right panel). Ionizable amino lipid DLin-MC3-DMA, helper lipid DSPC (phosphatidylcholine), polyethylene glycol-dimyristolglycerol (PEG-DMG) and cholesterol Adapted from Tam et al. [67].

LNPs have proven to be highly efficient nanocarriers of short-interfering RNAs (siRNAs) to hepatocytes *in vivo*. In 2018, Onpattro, a siRNA carrying LNP formulation, was approved by FDA. Onpattro performs by silencing the expression of transthyretin within the hepatocytes through delivering siRNA [69]. Recently, LNPs were used in COVID-19 vaccines to deliver mRNAs. Moreover, there are other mRNA vaccines that are currently under clinical trials to treat various diseases such as cancer and genetic diseases [70].

Understanding the therapeutic effect of anti-miR155 in the liver is ongoing research. Bala et al. transfected miR-155 inhibitor to RAW 264.7 macrophages by using lipofectamine transfection reagent [71]. Teng et al. successfully delivered antimiR-155 to the liver macrophages using baicalein nanorods [72]. Even though Zhang et al. used Lactosylated gramicidin-containing LNPs (Lac-GLN) to carry antimiR-155 for treating hepatocellular carcinoma [73], the lipid mixture did not contain ionizable lipid DLin-MC3-DMA. In this study, for the first time, we delivered antimiR-155 to inflammatory macrophages by using MC3 lipid-containing LNPs to alleviate the inflammatory response. In addition, as a natural alternative to LNPs, nanocarrier properties of extracellular vesicles (EVs) were investigated.

1.5.2. Extracellular Vesicles (EVs)

Extracellular vesicles (EVs) are heterogeneous membranous vesicles responsible for cell-to-cell communication. EVs can be originated from different cell types and the size of the EVs can change between 30nm to 2000nm in diameter. There are different EV populations, namely exosomes, microvesicles and apoptotic bodies, and exosomes are the smallest population (30-150 nm) among them (in **Figure 12**). Over the years, it has been demonstrated that exosomes play pivotal roles in physiological and pathological processes such as tissue repair, immune surveillance, and tumorigenesis, depending on their cargo. As a part of cell-to-cell communication, exosomes carry biologically active complex molecules such as mRNAs, miRNAs, cytoplasmic proteins, and lipids. Due

to their high biocompatibility and natural RNA-carrying properties, exosomes are attractive biological nanovesicle platforms for drug and gene delivery applications [74]. Therefore, delivery of microRNAs by naturally occurring RNA carriers is an alternative to lipid nanoparticles.

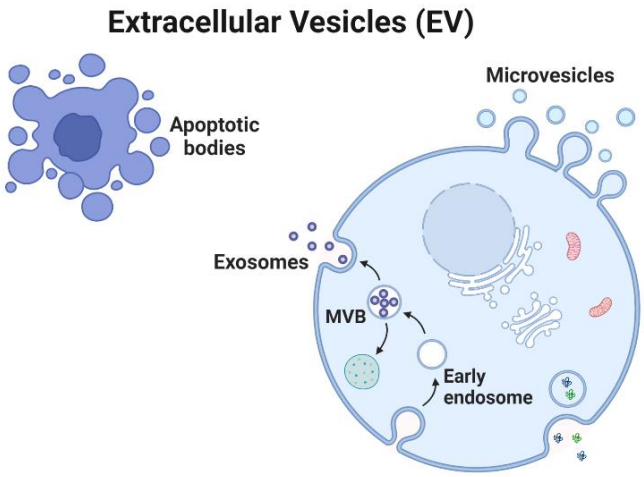

Figure 12: **Extracellular vesicles populations**. Created with BioRender.com

Mesenchymal stem cells (MSCs) are a type of adult stem cells and can be isolated from different tissues, including adipose tissue, umbilical cord, bone marrow, and dental pulp [75]. MSCs are able to produce components that can restore damages in tissues and mitigate immune response; therefore, they are appealing candidates for regenerative medicine and tissue engineering. In addition, MSCs can induce M2 macrophages to alleviate liver inflammation and exert their function through cytokines and hormones or the cargo carried by exosomes [75,76]. Initial reports suggested MSCs might play a crucial role in tissue repair; however, investigations have shown poor survival and low grafting capacity in injured tissue areas. Also, they carry the potential of malignant transformation, thus limiting MSC effectiveness in therapy [77]. Further studies showed the therapeutic effects of MSC were attributed to MSC-derived exosome rather than its trans differentiation property [78]. MSCs secrete more immunomodulatory exosomes than other cell types and exosomes produced from MSCs (Exo-MSCs) mimic the biological functions of the MSCs [51]. It was shown that exosomes derived from adipose MSCs (AMSCs) could alleviate inflammation by polarizing macrophages to the M2 phenotype through transactivating ARG-1 by exosome-carried active signal transducer and activator of transcription 3 (STAT3) [79]. In addition, exosomes derived from pre-activated AMSCs contain miRNAs involve in M2 polarization such as miR-34a-5p and miR146a-5p [80]. Considering the inherited anti-inflammatory potential of AMSC-derived exosomes, exploiting these exosomes as antimiR-155 carriers could boost the treatment efficiency.

2. Aim and Strategy of the Research

2.1. Aim and Objectives

As discussed, liver inflammation is the dominant driver of the pathogenesis of NASH. Therefore, targeting liver inflammation to treat NASH patients is a promising approach. Due to their regulatory roles in liver diseases, microRNAs are currently under the spotlight. Especially microRNA-155 (central regulator of inflammation) is a potent target for the alteration of liver inflammation.

The main objective of this project is to establish an antimiR-155 delivery platform to the liver macrophages to attenuate liver inflammation by reducing proinflammatory cytokine expressions. To achieve this, we compared two different nanocarriers namely lipid nanoparticles and exosomes. Up to now, no study has used ionizable lipid (MC3) containing lipid nanoparticles as a carrier of antimiR-155 to resolve liver inflammation. In addition, for the first time, we used AMSCs as a source of antimiR-155 carrying EVs. The sub aim of this study is to understand the characteristics of LNPs and EVs as nanocarriers to resolve liver inflammation.

To reach this aim, we have formulated different objectives,

- Understanding the role of microRNA-155 in inflammatory macrophages;
- Delivering antimiR-155 to manipulate miR-155 expression in macrophages and attenuate TNFα and IL-6 secretion;
- Engineering LNP formulation to find the optimum antimiR-155 delivery properties;
- Understanding the characteristics of LNPs and uptake behavior by different liver cells;
- Exploring the anti-inflammatory properties of AMSC-derived EVs and boosting this effect by transfecting them with antimiR-155.

2.2. Strategy

In this study, we first discussed NASH pathology and understand the roles of microRNAs in NASH development. Since liver inflammation is one of the critical drivers for the development of NASH, we focused on the main inflammation-related microRNA, miR-155. After explaining the role of miR-155 in liver inflammation, we discussed different nanoparticles, lipid nanoparticles, and EVs, as a delivery vehicle of antimiR-155, a microRNA therapeutic that silences overexpressed miR-155.

First, we delivered antimiR-155 using the commercially available transfection reagent HiPerFect; then, we explained its shortcomings. Following, we proposed LNPs as an alternative and less toxic RNA carrier and analyzed their uptake properties, effects on cell viability, and transfection efficiency. Lastly, the advantages and disadvantages of LNPs were analyzed according to our results.

In the last section of our experiments, we isolated EVs from AMSCs and exploited their innate immunosuppressive behavior. Moreover, we transfected AMSCs with antimiR-155 encapsulated HiPerFect in order to boost immunomodulation. Different M1 and M2 marker expressions were evaluated by qPCR.

3. Materials and Methods

3.1. Materials

Dulbecco's modified Eagle's medium (DMEM) (Lonza); fetal bovine serum (FBS) (Sigma-Aldrich); L-glutamine (Lonza) (Basel, CH); penicillin/streptomycin (pen/strep) (50U/ml Penicillin and 50µg/ml streptomycin, Sigma, St. Louis, MO, USA); Dulbecco's phosphate buffered saline (DPBS); Lipophilic Tracer DiD (Invitrogen); iScriptTM cDNA Synthesis Kit (Bio-Rad Laboratories, Inc.) (Hercules, CA, USA); RiboLock RNase Inhibitor, RevertAid Reverse Transcriptase, 5X Reaction Buffer, 10mM dNTP Mix (Thermo Scientific) SensiMixTM SYBR & Fluorescein Mix (Bioline Reagents) (London, UK); Bio-Rad CXF-384TM Real-Time System; PhD Ultra model pumps (Harvard Apparatus); staggered herringbone mixer chip (Microfluidic ChipShop); PEG-DMG, Cholesterol, 18:0 PC (DSPC) (Sigma-Aldrich); D-Lin-MC3-DMA (Hycultec); Cell Strainers, Smart Strainers (100µm) (MACS); Ultracentrifuge tubes (Amicon Ultra-4, 10k) (Millipore); RPMI 1640 with L-Glutamine (Capricorn Scientific) ; HiPerFect Transfection Reagent (Qiagen) ;Anti-miR-155: 5'-mA/ZEN/mCmCmCmCmUmAmUmCmAmCmAmAmUmUmAmGmCmAmUmUmA/3ZEN/(Mw=8,083.5) (Integrated DNA Technologies) ; mmu-miR-155-5-Stem-loop primer: GTTGGCTCTGGTGCAGGGTCCGAGGTATTCGCACCAGAGCCAACACCCCT, Forward primer: GGGGGTTAATGCTAATTGTGAT, Reverse primer :GTGCAGGGTCCGAGGT (Thermo Fisher).

3.2. Cell Culture

Mouse H5V endothelial cells, 3T3 fibroblast cells and AML12 hepatocytes were cultured in complete DMEM with 10% FBS and 1% penicillin/streptomycin. Mouse Raw 264.7 macrophages were cultured in RPMI with 10% FBS and 1% penicillin/streptomycin. All cells were cultured in a humidified incubator with 5% CO2 at 37 °C. After 24 h of incubation, 3T3 cells were starved for 8h and activated with 5ng/ml TGF-β for 24h before LNP treatment. AML12 cells were also starved 8h before LNP treatment to understand the effect of serum on the uptake of LNPs. Furthermore, AML-12 cells were incubated with 0.2 mM palmitic acid (PA) and 0.4mM oleic acid (OA) dissolved in isopropanol 24h prior to the treatment to understand the effect of fat accumulation on LNP uptake. For uptake studies, Raw 264.7 cells were stimulated with 100ng/ml LPS and 20ng/ml IFN-γ for the M1 proinflammatory phenotype, whereas 10ng/ml IL-4 and 10ng/ml IL-13 were used for M2 anti-inflammatory phenotype. In addition, for transfection studies, Raw 264.7 macrophages were stimulated 6h with 100ng/ml LPS and 20ng/ml IFN-γ for M1 and 10ng/ml IL-4 and 10ng/ml IL-13 for M2 phenotype.

3.3. HiPerFect Transfection

HiPerFect transfection reagent is used to transfect Raw 264.7 cells. 1 µg of anti-miR-155 was diluted in 100µl culture medium without serum per well. 5µl of HiPerFect transfection reagent was added to the diluted anti-miR-155 and mixed by vortexing. The mixture was incubated for 10 minutes at room temperature to allow the formation of transfection complexes. The complexes were then added in a drop-wise manner onto the cells. The plates were gently swirled to ensure uniform distribution. 400µl RPMI culture medium with 10% FBS and 1% penicillin/streptomycin was added to each well and cells were incubated for 24 h.

3.4. Lipid Nanoparticle Formulation

For the preparation of the lipid mix, ethanol containing ionizable lipid-MC3, phospholipid-DSPC, cholesterol, and helper lipid-DSPE-PEG at 50:10:38:1.5:0.5 mole ratio was prepared (**Table 1**).

Table 1: **Mol ratios of lipids used to formulate lipid nanoparticles**.

Lipid	% Mol ratio
DLin-MC3-DMA	50
DSPC	10
Cholesterol	38.5
DSPE-PEG	1.5
DiD	0.1 or 0.5

Total lipid concentration was arranged to either 15mM or 10mM. For uptake studies, the non-exchangeable tracer DiD was added to lipid mixtures. For the aqueous phase, a total of 50μg of RNA is dissolved in 100 mM sodium acetate (pH 4) buffer. The N/P ratio of antimiR-155 containing LNPs was arranged around 4. All the LNP formulations were produced using a microfluidic device with a flow rate ratio (FFR) of 3:1 (aqueous phase/lipid mix, total flow rate 4ml/min). Herringbone chip was used as a microfluidic chip for better mixing. The resulting LNP formulations were sterile filtered, dialyzed overnight against PBS (pH 7.4), and concentrated using 100K MWCO centrifugal filters at 3000g for 1h (Amicon® Ultra, Merck).

3.4.1. LNP Characterization

3.4.1.1. Particle Size and Zeta Potential

Particle size and polydispersity index (PDI) were measured via dynamic light scattering (DLS), and the surface charge was measured as zeta potential with Malvern zetasizer (Malver Instruments). Particle sizes and zeta potential were determined by diluting the samples 1:10 with PBS.

3.4.1.2. Encapsulation Efficiency

Encapsulation efficiency of RNA entrapped lipid nanoparticles was measured using PNI RiboGreen® Assay. After diluting formulated LNPs 1:10 with PBS, 15μl of the sample was used in the assay. The RNA encapsulation efficiency was calculated by comparing the RNA concentration in the presence and absence of Triton X-100 buffer. RNA concentration was calculated from its standard curve. After adding RiboGreen fluorescent dye, fluorescence was measured by a Varioskan Flash (Thermo Scientific, Waltham, MA, USA) with λex=500 nm, λem=525 nm.

3.5. Adipose Mesenchymal Stem Cell (AMSC) Isolation and Culture

AMSCs were isolated and prepared according to the procedure used by Chen et al. [81]. Shortly, adipose tissue surrounding the epididymis was carefully dissected from male mice and incubated for 15min in DMEM containing 10% FBS and 1% P/S. After incubation, adipose tissue was centrifuged at 200g for 7 min at 4 °C and digested in 2mg/mL collagenase Type 1 containing HBSS. After 60 min of incubation in thermaline shaker at 37 °C, the cell suspension was filtered through a 70µm cell trainer followed by a serial centrifuge at 400g for 10 min at 4 °C by using PBS as a resuspension solution. After the last centrifuge, cells were resuspended in 5 ml DMEM containing 10% FBS and 1%P/S and incubated in T25 flask overnight. The next day, the non-adherent cell was removed, and the medium was changed into a fresh one containing 10% FBS and 5 ng/mL FGF-2 (**Figure 13**). The third to fifth passages of ADSCs were used for the experiments.

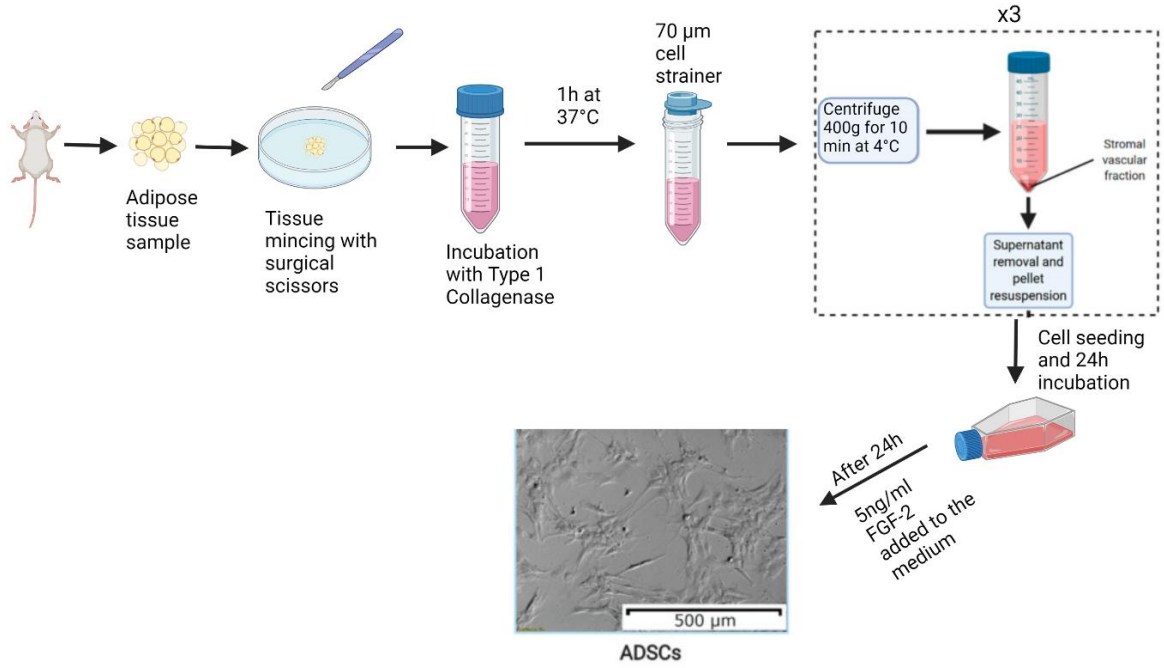

Figure 13: Schematic expression of the isolation of adipose derived mesenchymal stem cells. Adapted from Jankowski et al. [82].

3.6. Extracellular Vesicle Collection

For the EV collection, AMSCs were seeded 50.000 cells/ml or 100.000 cells/ml and starved for 48h using DMEM medium with no FBS addition. At the start of the starvation, 20ng/ml TNF-α and 20ng/ml IF-γ were added to the starvation medium. In addition, for the transfection studies, AMSCs were transfected with 2µg/ml antimiR-155 encapsulated HiPerFect Transfection reagent together with starvation medium. At the end of 48h, supernatants were collected and centrifuged at 300g for 10 min to remove cells followed by 2800g for 10 min to remove cellular debris. Supernatants were concentrated using Ultracentrifuge tubes (Amicon Ultra-4, 10k) (Millipore) at 2000g for 20 min. The size distribution and concentration of the collected EVs were analyzed using NanoSight NS500 Nanoparticle Tracking Analysis (NTA) (in **Figure 14**). Concentrated samples were used to treat Raw 264.7 macrophages for 24h.

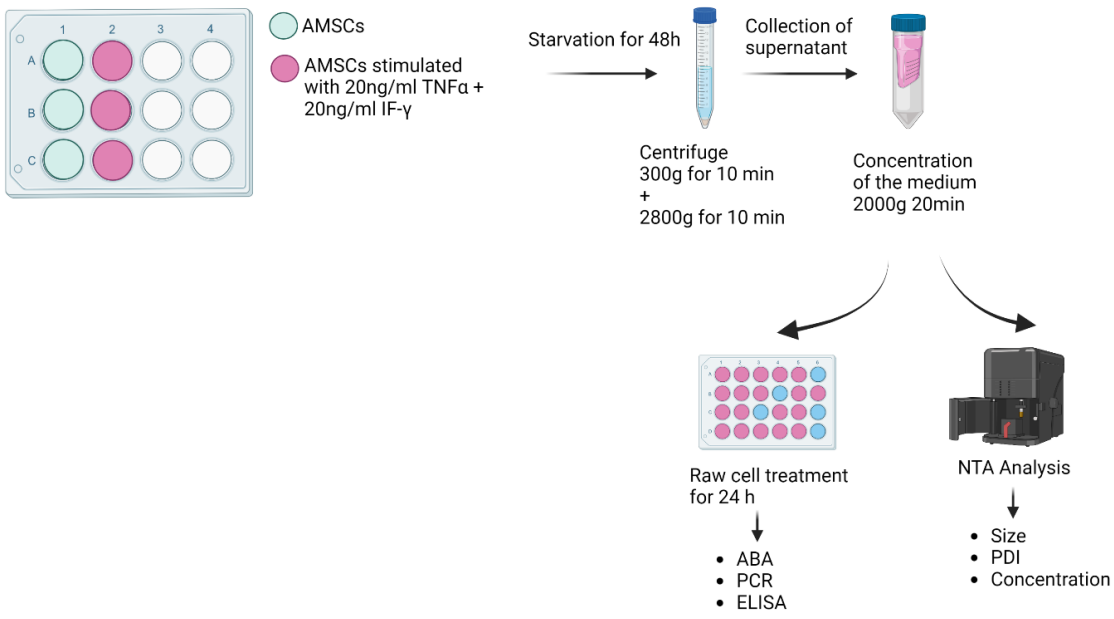

Figure 14: EVs collection and treatment of Raw 264.7 macrophages

3.7. Uptake Study

In order to understand the uptake properties of LNPs in different cells, lipophilic carbocyanine DiD fluorescent dye was encapsulated into LNP formulations. 4h after treatment with DiD-LNPs, cells were washed twice with PBS and detached. Cell aliquots were resuspended in 300 µL FACS buffer (2% FBS in PBS). The data were acquired using a BD FACS Aria II flow cytometer and the FACS Diva software and analyzed following the acquisition of at least 50,000 events after gating on viable cell populations.

3.8. Alamar Blue Assay

The metabolic activity of LNP-treated macrophages was measured using the Alamar Blue assay. The macrophages were plated in a 24-well plate and stimulated to drive M1 and M2 phenotypes, as mentioned previously. After 24h of incubation, the medium was removed, and the cells were washed once using 500 µL PBS. Simultaneously, 1x Alamar blue (AB) medium was prepared by dissolving 10x AB in RPMI medium containing 10% FBS and 1% P/S in a 1:10 ratio under dark conditions. After washing, the cells were incubated with 500 µL 1x AB medium for 4h. After incubation, 100µL medium of each well was collected in a 96 black bottom well plate and the absorbance of the medium was measured using the Victor 3 microplate reader. All samples were measured in duplicates.

3.9. qPCR

After 24h of treatment, all the cells were lysed using Trizol reagent according to the manufacturer's instructions. If not used directly, the RNA was stored at -80°C. After isolation, the RNA concentration and purity were measured with Nanodrop. Afterward, the RNA was diluted with distilled water to reach an equal concentration in every condition and cDNA was synthesized using the iScriptTM cDNA

Synthesis Kit, according to the manufacturer's instructions. After synthesis, the cDNA was again diluted to 10 ng/µL using distilled water. For the stem-loop cDNA synthesis, RevertAid First Strand cDNA Synthesis Kit (Thermo Fisher) was used. First, calculated water and RNA amount was added to the cDNA tubes and 1µl of mmu-miR155 stem-loop primer was added to each tube. Samples put in a water bath (65°C) for 5 min to allow the stem loop formation as can be seen in **Figure 15**. Reaction mix that contains 4 µl of 5X reaction buffer, 1 µl of RiboLock Rnase inhibitor, 2 µl 10mM dNTP Mix and 1 µl RevertAid M-MulV RT were added to each sample. If not used directly, the cDNA was stored at -20°C.

Realtime PCR was performed using GAPDH as a housekeeping gene. First, PCR master mix was prepared by adding 1.9µL distilled water, 0.05µL forward primer, 0.05µL reverse primer, and 4µL SYBR reagent per sample. All samples were measured in duplicates in 384-well plate. After the addition of 2µL of cDNA was added to the 384-well plate, 6µL of PCR master mix was added. The plate was sealed with a transparent lid and the wells plate was centrifuged for 1 min at 4000 rpm. Lastly, the qPCR was done according to a pre-configurated protocol, using the Bio-Rad CXF-384TM Real-Time System.

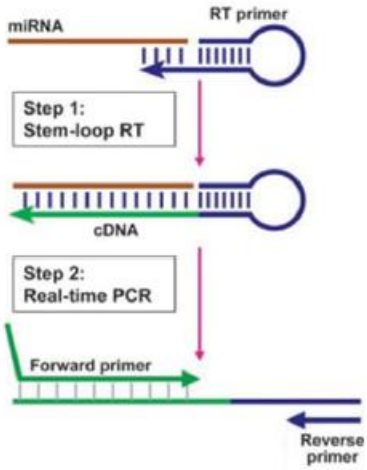

Figure 15: Schematic description of stem loop real-time quantification of miRNAs that includes two steps, stem–loop RT and real-time PCR. Stem–loop RT primers bind to at the 30 portion of miRNA molecules and are reverse transcribed with reverse transcriptase. Then, the RT product is quantified using qPCR that includes miRNA-specific forward primer and universal reverse primer [83].

3.10. ELISA

Levels of TNF-α and IL-6 in supernatants of Raw 264.7 cells after different treatments were measured by R&D System ELISA kit according to the manufacturer's protocol. 96-well plates were pre-coated with capture antibodies (Abs) overnight. Supernatants were added to the plates and samples were incubated at room temperature for 2 hours. Afterward, samples were washed, and detection Abs were diluted in PBS containing 1% BSA and added to the plates for 2 h at room temperature. After washing the plates, horseradish peroxidase (HRP)-conjugated streptavidin A was added for 20 minutes at room temperature. The HRP substrate TMB (3,3',5,5'-tetramethylbenzidine) was added to the plates, and the optical density of the color reaction was read on plate reader at 450 nm. Standard curves were generated and concentrations of cytokine in the culture supernatant were calculated.

4. Results and Discussion

4.1. MiR-155 Overexpression

The inflammatory process is a critical element of pathogenesis and the progression of NASH, where pro-inflammatory cytokine TNFα is the main driver. We analyzed the inflammation modulator miR-155 expression and inflammation markers IL-6 and TNFα levels in polarized Raw 264.7 cells.

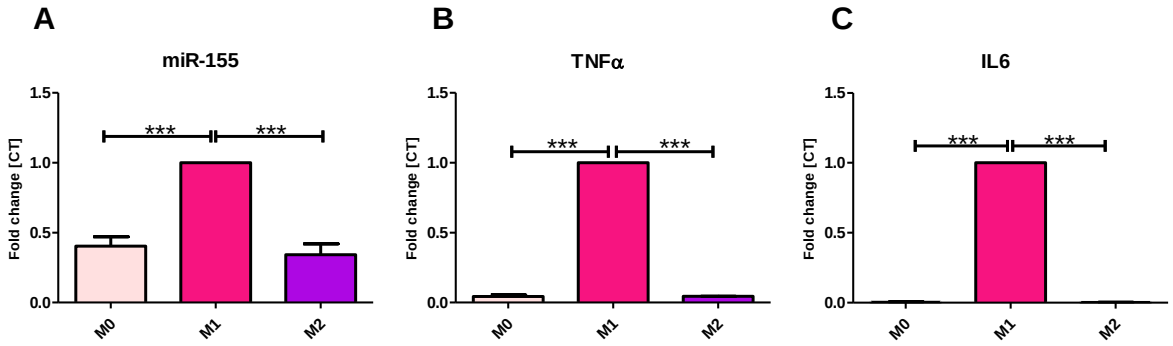

Figure 16: Gene expression levels of miR-155, TNFα and IL-6 in polarized macrophages. M0= Mouse Raw 264.7 with no treatment, M1= Mouse Raw 264.7 cells with 100ng/ml LPS and 20ng/ml IFN-γ treatment, M2= Mouse Raw 264.7 with 10ng/ml IL-4 and 10ng/ml IL-13 treatment for 6h. Data is normalized to GAPDH for all phenotypes. Significance was determined with the unpaired t-test, CI 95%, ***p<0.001

Our PCR results showed significantly overexpressed (2-fold) miRNA-155, (25-fold) TNFα, and (370-fold) IL-6 expression in M1-stimulated macrophages (in **Figure 16**). Overexpressed miR-155 targets inflammation regulators SHIP-1, SOCS-1, and BCL6 to promote the production of pro-inflammatory cytokines including TNFα and IL-6 [45]. Bala et al. found that activation of the NF-κB pathway through LPS stimulation causes an increase in the expression of miR-155. The upregulation of miR-155 exerts a stimulatory effect on TNFα release upon stimulation with LPS [53]. In miR-155 KO mice, LPS-induced increase in TNFα was attenuated compared to LPS-challenged WT mice [71]. Considering the established relation between miR-155, TNFα and IL-6, for silencing experiments, we continued to analyze miR-155 and TNFα as well as IL-6 levels.

4.2. AntimiR-155 Transfection with HiPerFect Transfection Reagent

After detecting the overexpressed miRNA-155 in pro-inflammatory macrophages, antimiR-155 was delivered to M1 macrophages via a commercially available HiPerFect transfection reagent, and changes in inflammatory response were measured by PCR.

First, Raw 264.7 cells were stimulated with 100ng/ml LPS and 20ng/ml IFN-γ treatment for 6h and treated with 2 µg/ml antimiR-155-HiPerFect complex. After 24h, the expression of miR-155 was measured using stem-loop qPCR as described in Section 3.9.

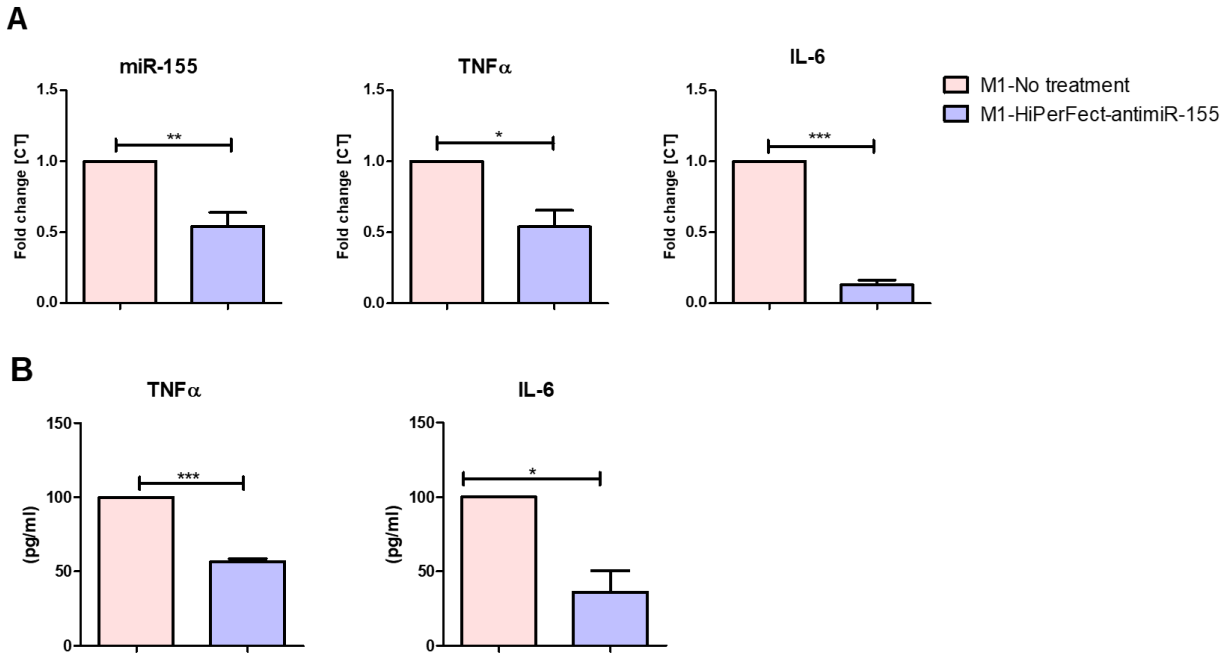

Figure 17: Expression levels of miR-155, TNFα and IL-6 were measured in M1 macrophages after antimiR-155-HiPerFect treatment (A) Gene expression levels of miR-155, TNFα and IL-6 after 24h antimir-155-HiPerFect treatment measured by qPCR. (B) Protein levels of miR-155, TNFα and IL-6 after 24h antimiR-155-HiPerFect treatment measured by ELISA. M1= Mouse Raw 264.7 cells with 100ng/ml LPS and 20ng/ml IFN-γ treatment for 6h. After 6h, 2 µg/ml antimiR-155 was added to the cells for 24h. Data normalized to GAPDH. Significance was determined with the unpaired t-test. *p<0.05, **p<0.01, ***, p<0.001.

Transfection of antimiR-155 successfully reduced (2-fold) the expression of miR-155 (in **Figure 17-A**). Downregulated miR-155 caused a significant reduction in the gene expression of TNFα (2-fold) and IL-6 (more than 7-fold) (in **Figure 17-A**). In addition, ELISA results showed a 2-fold reduction in TNFα and around 3-fold reduction in IL-6 protein levels after 24h of antimiR-155 delivery (in **Figure 17-B**). Thus, by delivering antimiR-155 encapsulated HiPerFect transfection reagent, we showed that our antimiR-155 is functional and effective in regulating miR-155 expression. In addition, we showed that the pro-inflammatory cytokine expression was significantly reduced upon antimiR-155 delivery, which shows the therapeutic potential of antimiR-155 for treating NASH.

4.2.1. Alamar Blue Results of AntimiR-155 Encapsulated HiPerFect Treatment

By interfering with the miR-155 expression, we were able to influence the pro-inflammatory phenotype (in **Figure 17**). Despite the transfection success of HiPerFect, commercial transfection reagents are not applicable for clinical treatments due to the cationic lipids that might be toxic to the cells [84]. To see the effect of HiPerFect on the viability of Raw 264.7 cells, we carried out an Alamar Blue experiment (in **Figure 18**).

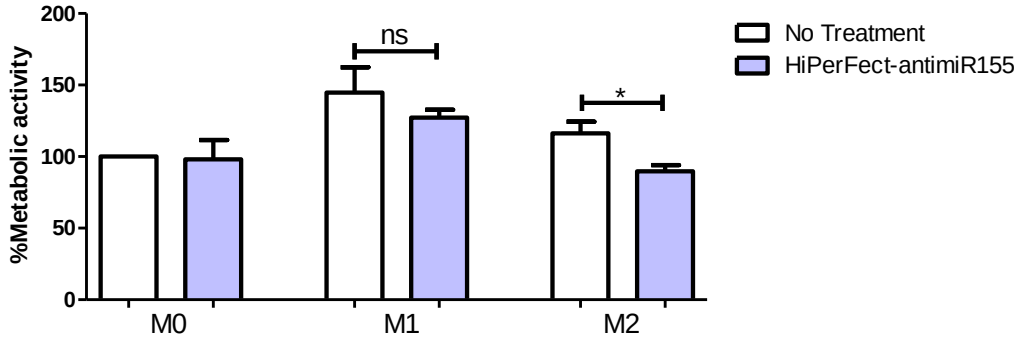

Figure 18: Metabolic activity of macrophages after the treatment with HiPerFect-antimiR-155 for 24h. M0= Mouse Raw 264.7 with no treatment, M1= Mouse Raw 264.7 cells with 100ng/ml LPS and 20ng/ml IFN-γ stimulated for 6h. All samples were normalized to M0 no treatment. Significance was determined with the unpaired t-test, CI 95%, * $p<0.05$

Even though no change in metabolic activity was observed in M0 macrophages, M1 and M2 macrophages showed a reduced metabolic activity which was significant in M2 macrophages. Thus, we set out to find an alternative carrier to transfection reagents. We suspected antimiR-155 itself might cause the reduction in metabolic activity; however, as we explained in Section 4.3.6., encapsulation of antimiR-155 did not change the metabolic activity of macrophages. After proving that antimiR-155 is efficiently binding its miR-155 target and reducing its expression, as a next step, we wanted to analyze the potential of lipid nanoparticles as an antimiR-155 carrier to liver macrophages. Due to the ionizable lipid components of LNPs, compared to the positively charged transfection reagents, higher tolerability was expected.

4.3. AntimiR-155 Transfection with LNPs

4.3.1. LNP Characterization

LNPs were produced according to Section 3.4. by using a microfluidic device and a microfluidic chip. To evaluate the average size and zeta potential of lipid nanoparticles, ζ-sizer was used. 15mM and 10mM lipid containing LNPs were produced together with either 0.1 mol% DiD or 0.5 mol% DiD lipophilic fluorescent dye. RiboGreen assay was used to determine the encapsulation efficiency of the LNPs.

4.3.1.1. ζ -sizer Results

Table 2: Size (as measured by DLS), polydispersity (PDI), surface charge (as measured by zeta potential)

Formulation	Average Size (nm)	PDI	Zeta Potential (mV)
Empty-LNPs (15mM)	109.4 ± 1.8	0.17 ± 0.042	-3.22 ± 0.09
0.1% DiD LNPs (15mM)	126.1 ±1.7	0.17 ± 0.02	-3.90 ± 1.03
0.5% DiD LNPs (10mM)	200.3 ± 2.581	0.12 ± 0.033	-2.51 ± 0.061
antimiR-155 LNPs (10mM)	142.8 ± 2.401	0.2 ± 0.027	-2.89 ± 0.246

The average size of empty LNPs (15mM) was around 110nm, whereas when DiD was incorporated, the size slightly increased to 125nm (in **Table 2**). When we reduced the lipid concentration, the size of the LNPs was increased up to 200nm. Particle size of the LNPs is determined by PEG lipid content. Higher PEG concentrations yield smaller LNPs [85]. Since we lowered the lipid concentration from 15mM to 10mM, total PEG concentration was also reduced which might the reason for bigger LNPs. On the other hand, when antimiR-155 was incorporated, the size was reduced to 142nm. The reason could be that the negatively charged RNA keeps the lipids closer to the core. The PDI of all the samples was between 12% to 20%, and the surface charge was neutral.

4.3.1.2. RiboGreen Assay Results

Determination of encapsulation efficiency (EE) is critical quality control for LNP production. RiboGreen assay was used to measure EE of antimiR-155 and scrambled RNA-loaded LNPs. For scrambled RNA-loaded LNPs, encapsulation efficiency was found to be 96.4%. Loading efficiency (LE) was 64.53% when RNA that was lost during the production due to dead volume was also considered. Even though high EE and LE were achieved with scrambled RNA-loaded LNPs, the EE of anti-miR-155 loaded could not be measured because the wavelength of the ZEN modifications of RNA with RiboGreen dye interfered. All calculations were made following the assumption that the EE of antimiR-155 loaded LNPs was the same as that of scrambled RNA-loaded LNPs (64.53%).

4.3.2. FACS Results of 15mM DiD Containing LNPs

Macrophages play pivotal roles in liver inflammation. They arise from circulating monocytes and depending on the microenvironment; they can become either M1 (classically activated) and M2 (alternatively activated) macrophages [86]. Therefore, targeting macrophages to resolve liver inflammation is a promising approach. To bring relevant therapies, liver microanatomy must be well understood.

The liver consists of parenchymal hepatocytes, Kupffer cells, liver sinusoidal endothelial cells (LSEC), dendritic cells (DC), liver-associated lymphocytes, and hepatic stellate cells (HSC) (described in **Figure 19**) [87]. The periportal region is where Kupffer cells are primarily found in the liver. When antigens or pathogens reach the liver through the portal vein, Kupffer cells are in a prime position to phagocytose and remove them. On the other hand, LSEC serve as a barrier between hepatocytes and macromolecules, or leukocytes present in the sinusoidal lumen. LSEC prevents direct interaction between passenger leukocytes and hepatocytes [88].

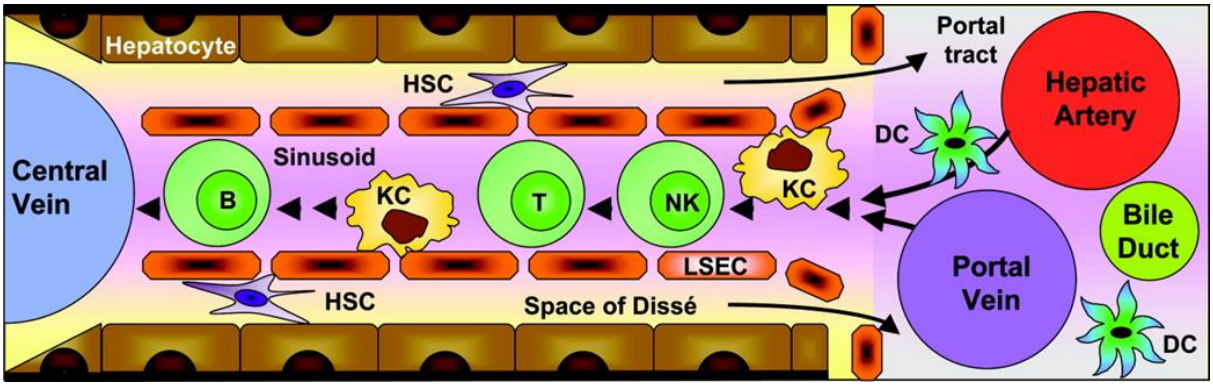

Figure 19: Microanatomy of the liver. Adapted from Racanelli et al. [87].

To understand the uptake of LNPs, they were loaded with fluorescent dye, DiD, and incubated with different liver cells. The uptake behavior of liver cells was analyzed using FACS. Mouse hepatocytes (AML-12), macrophages (RAW 264.7), fibroblast cells (3T3), and endothelial cells (H5V) cells were treated with 0.1 mol% DiD containing 15mM LNPs for 4h and DiD positive cells analyzed (in **Figure 20**).

Palmitic, oleic, and linoleic acids represent 70% of circulating FFAs. FFAs can enter the liver through portal circulation and contribute to the formation of NASH by serving as ligands for TLR4. [6] To elucidate the uptake behavior of healthy vs. NASH hepatocytes, we tested uptake in normal and palmitic acid (PA)/oleic acid (OA) treated hepatocytes.

In normal liver, HSCs are responsible storing of vitamin A metabolites. Following liver injury or inflammation, HSCs are activated and become proliferative, fibrogenic, and contractile myofibroblasts, leading to liver fibrosis. Different elements initiate HSC activation, including Kupffer cell infiltration or platelets that mediate platelet-derived growth factor (PDGF), transforming growth factor β1 (TGFβ1), and epidermal growth factor (EGF) [89]. In this study, we analyzed the LNP uptake from mouse liver fibroblasts; in addition, we either starved or starved and activated 3T3 cells with TGF-β and investigated the effect of different treatments on the LNP uptake.

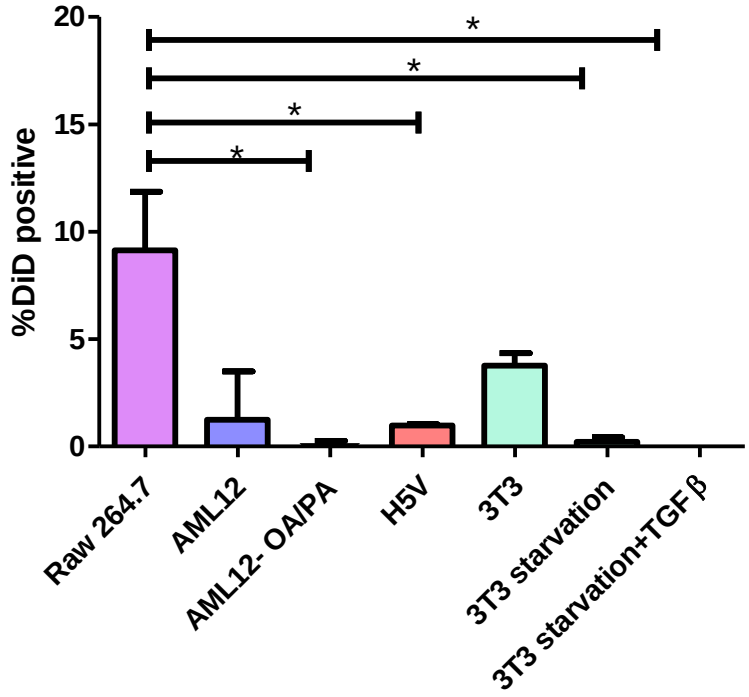

Figure 20: DiD positive cell percentage after the treatment with 0.1 mol% DiD containing 15mM LNPs. Raw 264.7 mouse macrophage cells with no treatment, AML12-OA/PA= AML12 cells activated with 0.2 mM palmitic acid (PA) and 0.4mM oleic acid (OA), for starvation, cells cultured in FBS depleted medium for 24 h together with LNP treatment. 3T3=fibroblast cells stimulated with 5ng/ml TGF-β, and H5V=endothelial cells. Significance was determined with the unpaired t-test, CI 95%, * $p<0.05$.

Raw 264.7 macrophages showed the highest uptake compared to the other cell types and this can be attributed to their phagocytosis function. However, due to the high variation in DiD positive cells, we did not detect a significant difference between macrophages and hepatocytes. Since hepatocytes occupy 80% of the total liver tissue, higher uptake from macrophages and lower uptake from hepatocytes are desirable for liver inflammation treatment. Moreover, it is known that miR-155 is also overexpressed in hepatocytes after MCD-induced steatohepatitis and plays complex roles in liver inflammation and fibrosis. Csak et al. demonstrated that miR-155 deficient mice showed attenuated liver fibrosis and reduced collagen expression [51]. Thus, delivering antimicroRNA-155 to hepatocytes and fibroblasts would further reduce the overexpressed miR-155 in total liver and contributes to the treatment of NASH.

Upon exposure to serum proteins, protein corona formation occurs around LNPs that affects the uptake of the particles [90]. In starved 3T3 cells, we do not observe any uptake compared to non-starved 3T3 cells. Thus, we can say that the uptake of LNPs by fibroblast cells depends on the serum proteins.

In vivo delivery of LNPs leads to accumulation in 3 main cell types, KC, hepatocytes, and LSEC, in a time and dose-dependent manner [91]. LSECs are located near Kupffer cells and play crucial roles in sequestering LNPs by their endocytic activities. Therefore, we were also expecting high uptake from H5V cells. However, we observed higher LNP uptake from 3T3 cells than from H5V cells. The reason might be the technical problems we faced during FACS. H5V cells had to wait longer than 3T3 cells before the FACS measurement. As a result of the long waiting time, aggregation of DiD was observed on the bottom of the tubes that contain the H5V cells. If the internalized DiD leaks out from the cells

during the waiting time, it could be the reason for the lower signal. Therefore, we redid this experiment in Section 4.3.5.

Many LNP delivery platform often assumes delivery mainly to hepatocytes [69]. However, our *in vitro* data and other biodistribution studies [92,93] show that the uptake of MC3-LNPs is higher in macrophages compared to other cell types in the liver. In addition, liver inflammation can lead to the activation of fibroblast cells which cause fibrotic material deposition. This deposition eventually inhibits the transport of particles to hepatocytes. This characteristic is vital for our project because macrophages are the key players in inflammation, and with our LNP formulation, we are able to target liver macrophages.

4.3.3. qPCR Results of 15mM Empty LNPs

Macrophages are the major producer of TNFα, and its overexpression is associated with inflammatory diseases [94]. Due to its regulatory effect on inflammation, it is essential not to induce TNFα levels while targeting inflammation, especially when we aim to reduce the TNFα expression by delivering antimiR-155 [52]. With this aim, we measure the expression level of TNFα after treating M0, M1, and M2 macrophages with 15mM empty LNPs (in **Figure 21**).

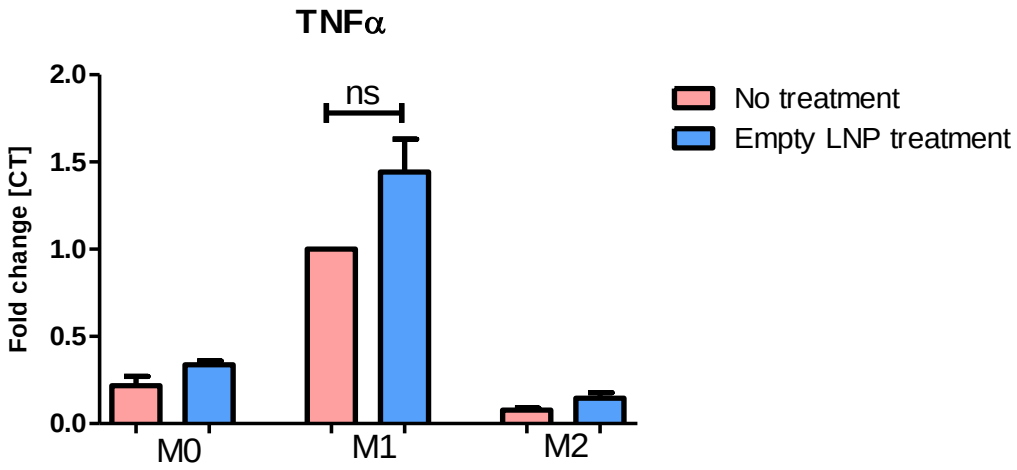

Figure 21: Expression of TNFα after 24h of 15mM empty LNP treatment. M0= Mouse Raw 264.7 with no treatment, M1= Mouse Raw 264.7 cells with 100ng/ml LPS and 20ng/ml IFN-γ treatment, M2= Mouse Raw 264.7 with 10ng/ml IL-4 and 10ng/ml IL-13 treatment for 24 h. Significance was determined with the unpaired t-test, CI 95%, * p<0.05, ** p<0.01.

After 24 h of treatment, enhanced TNFα expression was observed with 15mM LNP treatment. Even though it is not a significant increase, it is still undesirable for the purpose of this study. After observing TNFα induction, we decided to evaluate the effect of empty LNPs on macrophage viability using the Alamar Blue assay.

4.3.4. Alamar Blue Assay Results of 15mM Empty LNPs

It is known that upon LPS activation, the expression of miR-155 is enhanced [47]. Therefore, delivering antimiR-155 would directly decrease the miR-155 expression and alleviate inflammation. Undoubtedly, choosing the right nanocarrier is critical since the nanocarrier itself should not induce inflammation or reduce viability in order to have an effective therapeutic response. In light of our hypothesis, M0, M1, and M2 macrophages were treated with empty LNPs (15mM lipid concentration) that do not contain any RNA. According to our microscope observations, metabolic activity correlates with viability. While M0 and M2 macrophages did not show any reduction in metabolic activity, a significant change was observed in M1 macrophages (in **Figure 22**).

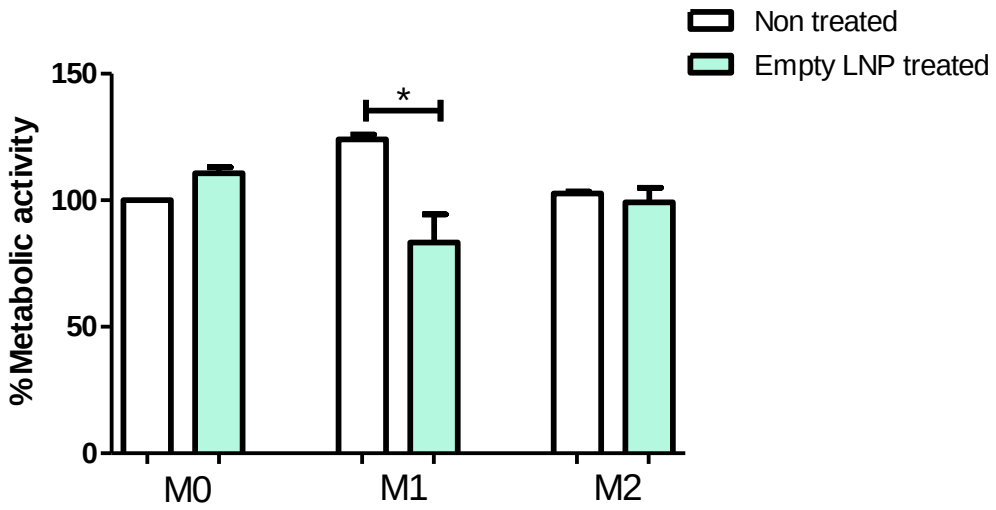

Figure 22: Alamar blue assay analysis of M0, M1 and M2 RAW macrophages after 15mM empty LNP treatment. M0= Mouse Raw 264.7 with no treatment, M1= Mouse Raw 264.7 cells with 100ng/ml LPS and 20ng/ml IFN-γ treatment, M2= Mouse Raw 264.7 with 10ng/ml IL-4 and 10ng/ml IL-13 treatment for 24 h. Significance was determined with the unpaired t-test, CI 95%, * $p<0.05$.

Despite being used in an FDA-approved drug, Onpattro (Patisiran), Dlin-MC3-DMA (MC3), for chronic therapies might cause undesirable side effects. These side effects are mostly due to the slow biodegradation of MC3. Sabnis et al. demonstrated that MC3-based LNPs caused elevated alanine transferase (ALT) and aspartate aminotransferase (AST) levels (indicators of liver damage) and evidence of necrosis in rats compared to ester-modified lipid-containing LNPs Thus, it is logical to assume that we observed reduced metabolic activity in M1 macrophages due to the high MC3 concentration. Hence, for the upcoming experiments, 10mM of lipid mix will be used instead of 15mM to produce LNPs.

4.3.5. FACS Results of 10mM DiD Containing LNPs

15mM of LNP concentration showed unwanted toxicity effects on Raw macrophages and caused enhanced TNFα expression (in **Figure 21**). Therefore, as a next step, instead of 15mM LNPs, we produced 10mM LNPs and encapsulated 0.5 mol% DiD to observe whether uptake behavior is affected by the reduced concentration of the lipids.

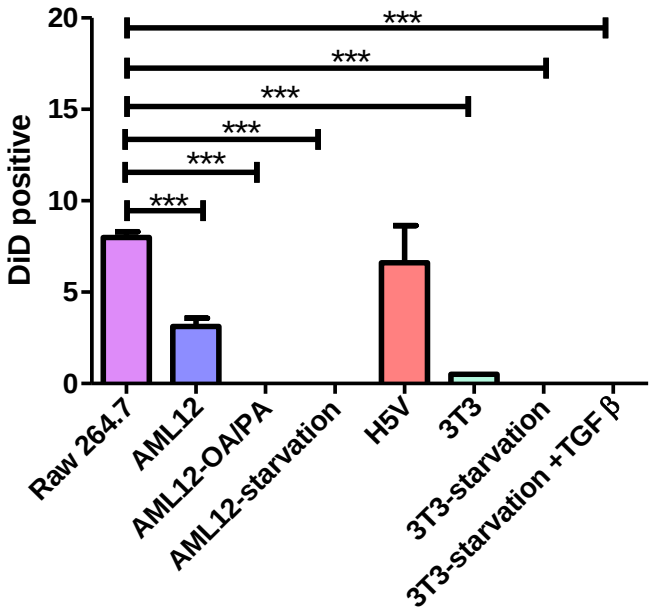

Figure 23: DiD positive cell percentage after the treatment of mouse liver cells with 0.5 mol% DiD containing 10mM LNPs. Raw 264.7 mouse macrophages with no treatment, AML12-OA/PA= AML12 cells activated with 0.2 mM palmitic acid (PA) and 0.4mM oleic acid (OA), for starvation, cells cultured in FBS depleted medium for 24 h together with LNP treatment (4h). 3T3=fibroblast cells stimulated with 5ng/ml TGF-β, and H5V=endothelial cells. Significance was determined with the unpaired t-test, CI 95%, * p<0.05, **p<0.01, ***, p<0.001

Correlating with the first uptake results, we again observed the highest uptake from Raw macrophages with a lower error bar, which might be due to the higher amount of DiD in the formulation (**Figure 23**). We also observed a significant difference in the uptake behavior of LNPs by AML12 hepatocytes compared to Raw cells. Similar to 15mM LNPs, fat-laden hepatocytes showed no uptake of 10mM LNPs. During the formation of NASH, free fatty acids and triglyceride accumulate in hepatocytes [6]. Thus, we expect less LNP uptake from hepatocytes in a NASH liver compared to a healthy liver. To confirm this, further *in vivo* studies are necessary. In addition, we starved the hepatocytes 24h before the uptake study to understand the effect of serum proteins on the uptake of LNPs. Apolipoprotein E (apoE) in the serum adsorbs onto the surface of LNPs. This binding promotes the uptake by hepatocytes through the low-density lipoprotein receptor (LDLr) expressed on hepatocytes' surface [93]. As expected, when we incubated the AML12 with no FBS-containing medium, there was no uptake of LNPs.

KCs together with LSECs makes up the hepatic reticuloendothelial system (RES) whose major function is to scavenge macromolecular waste and pathogens from blood in order to maintain blood homeostasis [95]. Therefore, high uptake from endothelial cells (H5V) was expected *in vitro*. However, to conclude the uptake behavior of different liver cells, further in vivo studies are necessary. Moreover,

3T3 fibroblast cells have lower uptake than H5V endothelial cells, while starved or activated 3T3 cells again showed no uptake of LNPs.

At this stage, our LNP formulation is not targeting specifically macrophages, and it exploits the passive targeting of the liver. Thus, off-targets are inevitable. In order to target specifically macrophages, LNP formulations can be modified with anti-CD163 monoclonal antibody (mAB) to target macrophage-specific surface marker CD163 [96]. In addition, Pattipeiluhu et al. showed that the uptake of negatively charged LNPs was higher in KCs and LSECs mediated by stabling-2 receptors compared to LDL receptor-mediated uptake of hepatocytes [93]. Thus, changing the surface charge of LNPs from neutral to negative might further increase the uptake from macrophages.

4.3.6. Alamar Blue Assay Results of 10mM LNPs

Next, we produced 10mM lipid containing empty LNPs or antimiR-155 containing 10mM LNPs and treated our cells (2µg/ml antimiR-155 concentration) for 24h after adding different polarization stimuli.

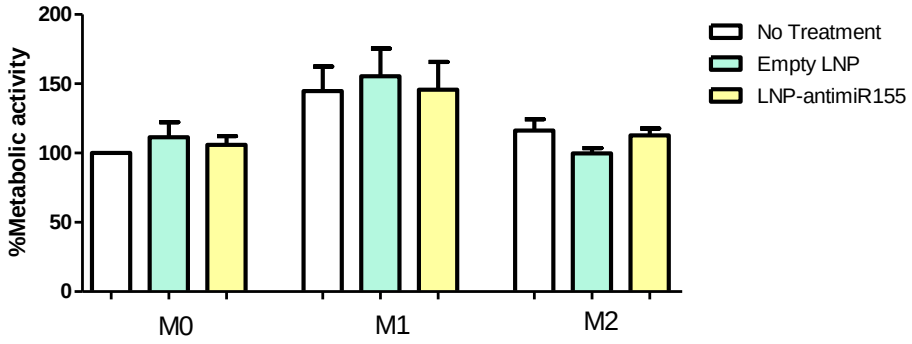

Figure 24: Alamar blue assay analysis of M0, M1 and M2 RAW macrophages after 10mM LNP treatment. M0= Mouse Raw 264.7 with no treatment, M1= Mouse Raw 264.7 cells with 100ng/ml LPS and 20ng/ml IFN-γ treatment, M2= Mouse Raw 264.7 with 10ng/ml IL-4 and 10ng/ml IL-13 treatment for 24h. LNP-antimiR-155 contains 2µg/ml antimiR-155. LNP-antimiR-155 incubated with M0-M1 and M2 cells for 24h.

Figure 24 shows that 10mM empty LNPs do not significantly affect the metabolic activity of liver macrophages. Compared to 15mM lipid concentration, 10mM LNPs showed higher tolerability by macrophages. These results were in accordance with our microscope observations. Moreover, antimiR-155 incorporation did not affect the viability of the cells. Therefore, 10mM lipid concentration was found to be the ideal concentration to transfect the cells with antimiR-155**.**

4.3.7. qPCR Results of 10mM AntimiR-155 Encapsulated LNPs

Next, M1 macrophages were treated with antimiR-155 encapsulated 10mM LNPs for 24h, and the changes in the gene expression of miR-155, TNFα, and IL-6 were measured by qPCR. All gene expressions were significantly reduced after the treatment (**Figure 25**).

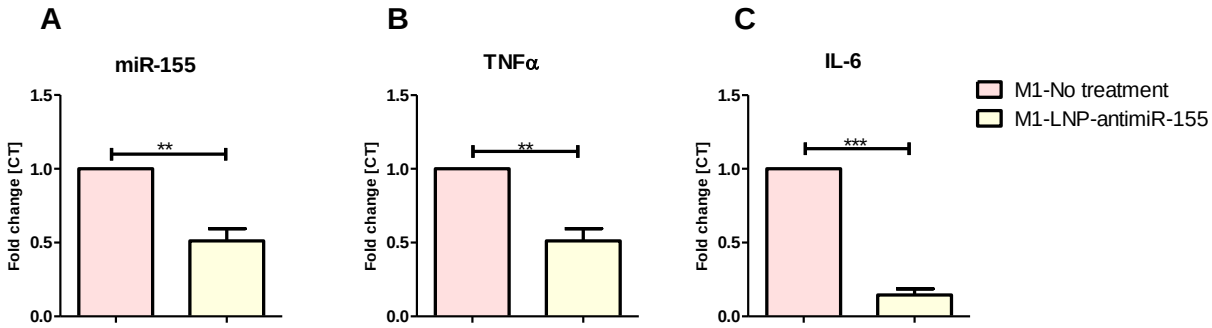

Figure 25: Gene expression of miR-155, TNFα and IL-6 were measured in M1 macrophages after LNP-antimiR-155 treatment. M1= Mouse Raw 264.7 cells with 100ng/ml LPS and 20ng/ml IFN-γ treatment for 6h. After 6h, 2 μg/ml antimiR-155 was added to the cells for 24h. Data normalized to GAPDH. Significance was determined with the unpaired t-test, CI 95%, *p<0.05, **p<0.01, ***, p<0.001.

Overall miR-155 expression was reduced 2-fold after antimiR-155 delivery with LNPs. Reduction in miR-155 expression led to a 2-fold decrease in TNFα and a more than 6-fold decrease in IL-6 expression. As a result, 10mM MC3 containing LNPs was found to be less toxic than HiPerFect while showing the same transfection efficiency.

4.3.8. ELISA

The miR-155 not only increases the gene expression of TNFα but also enhances its mRNA half-life and translation. [32,53] After showing anti-miR-155 delivery to the M1 macrophages reduced the gene expression of TNFα and IL-6 (**Figure 25**), from the same samples, supernatants were collected to measure TNFα and Il-6 protein levels by ELISA. A reduction in mRNA levels of TNFα and IL-6 was observed after antimiR-155 delivery (in **Figure 26**).

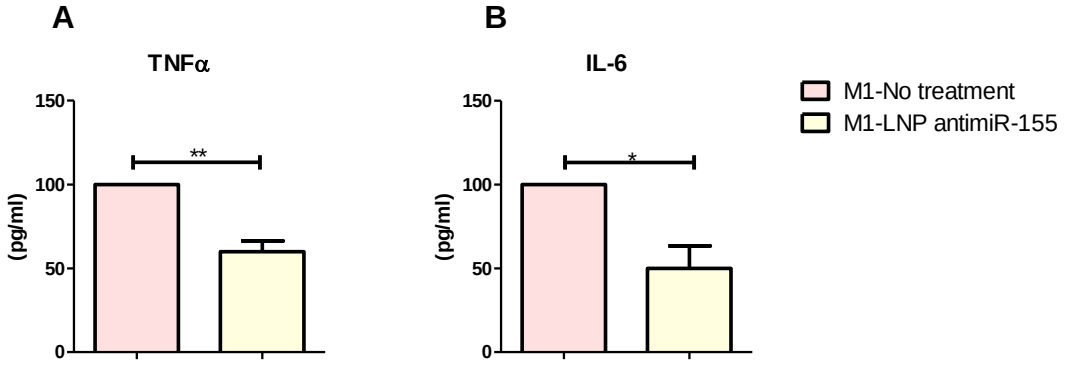

Figure 26: ELISA results of LNP-antimiR-155 treated M1 macrophage. TNFα and IL-6 protein levels were measured in supernatants by ELISA after collection of the medium. Significance was determined with the unpaired t-test, CI 95%, *p<0.05, **p<0.01, ***, p<0.001.

As a result, delivering antimiR-155 attenuated pro-inflammatory cytokine secretion of TNFα and IL-6, both gene expression and protein level; however, it does not entirely block their production. To further improve the decrease in the secretion of TNFα, a dual delivery approach can be taken. Pentoxifylline is a drug that inhibits TNFα, and it can be used for the treatment of severe alcoholic hepatitis [97]. Together with antimiR-155, Pentoxifylline can be incorporated into LNPs to increase its efficiency further and attenuate liver inflammation. Moreover, delivering another microRNA together with antimiR-155 could help to tackle inflammation by targeting various inflammatory pathways. Anti-inflammatory miR-146a overexpressed after LPS treatment in macrophages and suppressed the pro-inflammatory response. MiR-146a serves as a regulatory negative feedback loop to suppress NF-κB activity by silencing IRAK1 and TRAF6 and resolving inflammation [98].

4.4. AntimiR-155 Transfection with Extracellular Vesicles (EVs)

As discussed in the introduction, new therapies that could suppress the immune response without causing detrimental side effects are urgently necessary. Using lipid nanoparticles, we were able to reduce immune response by delivering anti-miRNA-155 and lowering the expression of miR-155, TNFα, and IL-6 in macrophages. However, the administration of synthetic lipids like MC3 are threatening due to biodegradation concerns. Even though antimiR-155 delivery with LNPs created a potent anti-inflammatory effect on M1 macrophages, in a multiple injection scenario, LNPs might create toxicity issues. Hence, we also experimented with EVs in order to overcome the shortcomings of LNPs.

Previous studies showed that MSCs are effective for tissue repair, regeneration as well as inflammation [99]. Nonetheless, their age-dependent nature [75] and, most importantly risk of unwanted differentiation of transplanted MSCs raise some concerns in their clinical applications [100]. Subsequently, research presented that the immunomodulatory effect of MSCs was attributed to the EVs, mostly exosomes secreted from them [77,101]. Hence, in this set of experiments, we exploited MCS-derived EVs as a natural alternative to LNPs and analyzed their immunosuppressive behaviors.

4.4.1. Extracellular Vesicle (EV) Preparation and Isolation

AMSCs were seeded 50.000 cells/ml and starved for 48h. Starvation is necessary to prevent the intervention of FBS-derived EVs with AMSC-derived ones. For some cells, we added stimulation with pro-inflammatory cytokines and called them stimulated AMSC throughout the experiments. Domenis et al. found that when AMSCs were treated with inflammatory cytokines, they showed immunosuppressive and anti-inflammatory potential by upregulating several genes involved in immunomodulation [80]. Thus, we also used stimulated AMSCs to boost the immunosuppressive behavior of AMSCs. We added 20ng/ml TNF-α and 20ng/ml IF-γ to the starvation medium for stimulation.

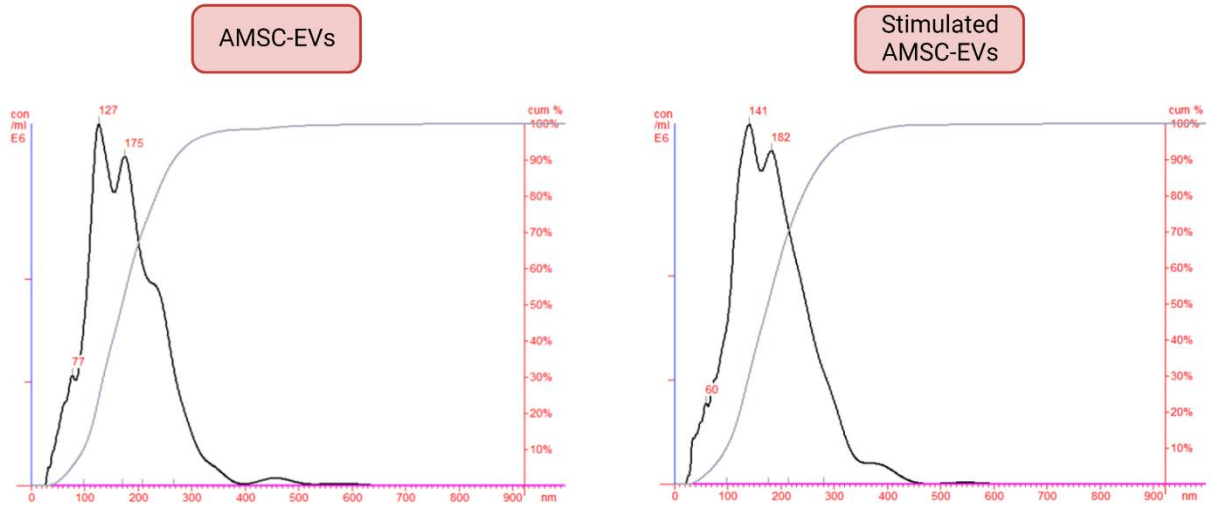

Figure 27: Concentration graphics of AMSC derived EVs. Y axis of the graphic represent the concentration of the EVs, and the X axis represent the size distribution. NTA was used to measure the concentration and the size distribution.

After incubation, the medium was collected and concentrated. Due to our time limitations, we could not isolate exosomes from EVs, instead we used the concentrated EVs to treat the M1 macrophages. NTA analysis showed a heterogeneous population (in **Figure 27**). Despite the heterogeneity, the highest concentration of the EV population was found at 127nm for AMSC-EVs and 141nm for stimulated AMSC-EVs, which correlates with the size of exosomes.

Table 3: **Characterization results of AMSC derived EVs by NTA.** EVs were collected from total 3 wells that contains 50.000 AMSC each. SD: standard deviation

Sample	Mean size [nm]	Mode [nm]	SD [nm]	Total concentration [particles/ml]
AMSC-EVs	180	127	74	5.25E+09
Stimulated AMSC-EVs	185	141	74	5.69E+09

The mean size of AMSC-EVs was 180nm, while it was 185nm for stimulated EVs. Therefore, we can say that stimulation of AMSCs did not affect the average size of the EVs (in **Table 3**). In addition, total concentration did not change significantly. The concertation of AMSC-EVs was 5.25E+09 particles/ml whereas the concentration of stimulated AMSC-EVs 5.69E+09 particles/ml. However, it was observed that at the end of the starvation period, AMSCs had around 50% confluency when they were seeded 50.000 cells/ml. According to the literature, the pronounced effect after exosome treatment was reached when the exosome concentration was around 7.6±2.6+E9 [80]. To see the real effect of starvation on AMSCs and increase the treatment effect, we decided to seed 100.000 cells/ml for the next experiment and total concentration of EVs was doubled.

4.4.2. Alamar Blue Results

MSC-derived exosomes do not have the major histocompatibility complex (class I and II) that enable them to evade immune rejection after transplantation. The absence of these complexes can cause low immunogenicity [80]. Hence, as a next step, we treated M1 macrophages with concentrated AMSC-EVs and stimulated AMSC-EVs to observe the toxicity effect. As a negative control, the same amount of starvation medium without any cell treatment was concentrated using the same process.

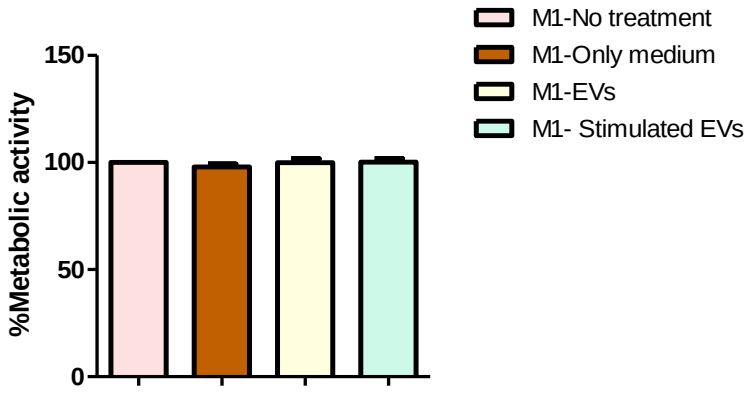

Figure 28: Alamar Blue assay results of Raw cell treated with AMSC-derived EVs for 24h. AMSCs starved with or without 20ng/ml TNF-α and 20ng/ml IF-γ stimulation for 48h. Medium was collected, concentrated. Raw cells were treated with concentrated EVs for 24h and they stimulated 6h with 100ng/ml LPS and 20ng/ml IFN-γ for obtaining proinflammatory M1 macrophages. Only medium sample was concentrated starvation medium that did not used for any cell treatment. All treatments are normalized to M1. Significance was determined with the unpaired t-test.

Raw cells were treated with the EVs for 24h, and the Alamar Blue assay was carried out. Stimulated or non-stimulated EVs did not show any reduction in the metabolic activity of the cells (In **Figure 28**), which is in accordance with the literature [80].

4.4.3. PCR Results

EVs carry different cytokines, growth factors, signaling lipids, mRNAs, and regulatory miRNAs to exert their biological effects. Depending on the cargo molecules, EVs can act as a modulatory of the immune response, promote an anti-inflammatory phenotype, or reduce pro-inflammatory cytokines produced by macrophages [75]. During NASH progression, the primary inflammatory cytokines generated by M1 macrophages are TNFα, IL-6, and IL-1β, and levels of these cytokines were reported to be elevated in NASH patients [12,13]. AMSC-derived exosomes have the ability to reduce inflammation by reducing pro-inflammatory markers and enhancing anti-inflammatory ones [101]. Therefore, therapeutically these exosomes carry the potential to be used in the treatment of NASH.

In our study, AMSC-derived EVs were collected, as explained in Section 4.4.1. Shortly, M1 macrophages were treated with concentrated EVs for 24h and the expressions of M1 and M2 markers were measured using qPCR. Surprisingly, expression of TNFα did not show any observable decrease after treatment with EVs or stimulated EVs. (**In Figure 29-A**). Zhao et al. demonstrated that preincubation with exosomes from AMSCs reduced the inflammatory responses of macrophages activated by LPS and IFN-γ, as observed by the significantly lower levels of TNF-α [79]. Contradictory to this study, TNF-α levels were constant after our EV treatment. One reason could be the low concentration of EVs. Since AMSCs confluency could not reach sufficient levels due to the low number of seeded cells, we may need higher concentrations to be able to observe a significant reduction in TNFα secretion. In addition, we also do not observe any reduction in IL-6 expression (in **Figure 29-C**). Stimulated EVs showed higher expression than non-stimulated EVs. The reason could be the residuals of pro-inflammatory cytokines. During the concentration process, even though we removed most of the medium along with the stimuli, with ultrafiltration, it is impossible to remove all the medium.

In addition, treatment with EVs did not affect the expression of IL-1β, whereas stimulated-EVs significantly lowered (3-fold) its expression compared to M1 macrophages (**in Figure 29-B**). IL-1β promotes liver steatosis and inflammation by signaling through the IL-1 receptor [12] and it is an important target for reducing the inflammatory response. We were expecting to see the downregulation after EVs treatment as well as stimulated EV treatment. However, we only observed a reduction with stimulated EVs. Domenis et al. stimulated AMSC-derived exosomes with different concentrations of TNF-α and IF-γ and observed profile changes in cargo miRNA levels. After the stimulation, anti-inflammatory miR-34 and miR-146 were overexpressed compared to non-stimulated controls [80]. It is also known that miR-146 is associated with IL-1β suppression [102]. Thus, maybe the miR-146 that is carried by stimulated EVs caused the observed reduction in IL-1β expression.

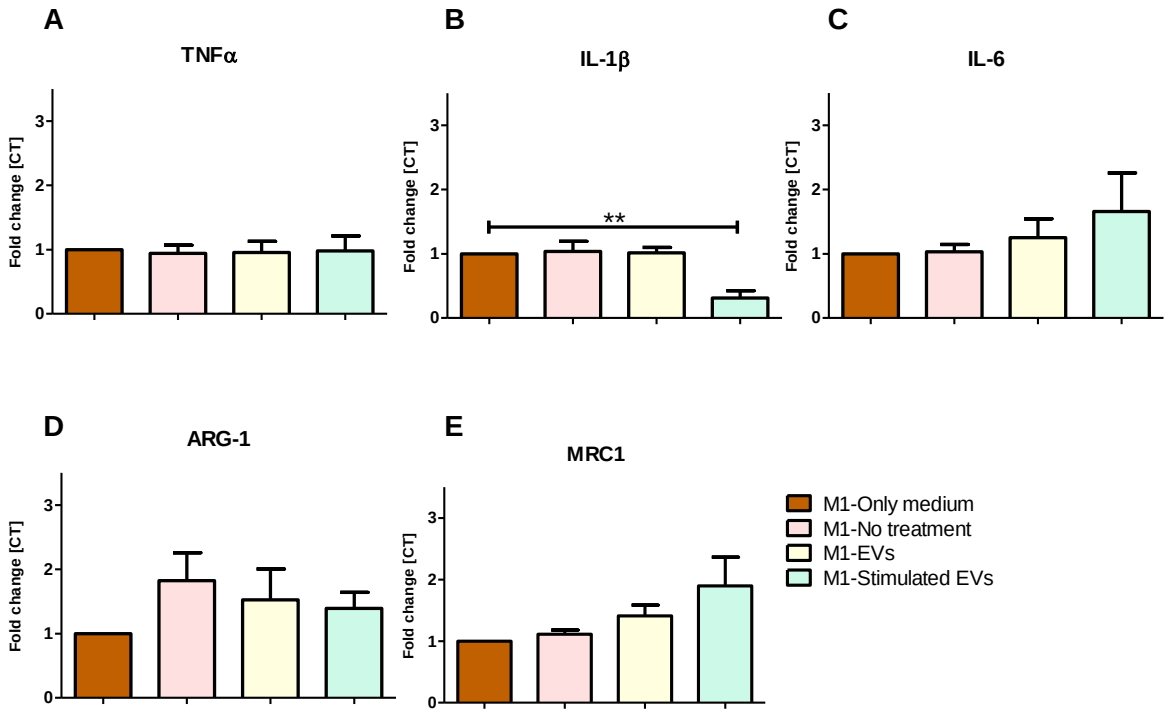

Figure 29: Gene expression levels after EV treatment of Raw macrophages. AMSCs starved with or without 20ng/ml TNF-α and 20ng/ml IF-γ stimulation for 48h. Medium was collected, concentrated. Raw cells were treated with concentrated EVs for 24h and they stimulated 6h with 100ng/ml LPS and 20ng/ml IFN-γ for obtaining proinflammatory M1 macrophages. Only medium sample was concentrated starvation medium that did not used for any cell treatment. All genes normalized to GAPDH. Significance was determined with the unpaired t-test, CI 95%, * $p<0.05$, ** $p<0.01$.

Apart from M1 markers, ARG1 and MRC1 gene expression levels were also measured to understand the effect of EV treatment on M2 markers. Zhao et al. treated obese mice with AMSC-derived exosomes, and as a result, obesity was reduced, and hepatic steatosis was alleviated. It was found that AMSC-exosomes were rich in active STAT3 and preincubation with these exosomes caused overexpression of ARG-1 in M1 macrophages [79]. Therefore, we checked STAT-3 mediated expression of both ARG-1 and MRC-1 [103]. Both genes showed no significant increase, and the treatment effect was not pronounced. Non-stimulated and stimulated EV treatment increased the expression of MRC1 insignificantly. The reason that we could not observe significant expression might be due to the low concentration of the EVs.

4.4.4. AntimiR-155 Transfection of AMSCs and Isolation of EVs

The next step was to double the amount of seeded AMSCs and transfect them with anti-miR-155 using HiPerFect. AMSCs were seeded 100.000 cells/ml and starved for 48h. To activate AMSCs with inflammatory factors, 20ng/ml TNF-α and 20ng/ml IF-γ were added to the starvation medium. Moreover, during starvation, each well was treated with 2µg/ml anti-miR-155 containing HiPerFect transfection reagent. After 48h, the medium was collected from different treatment groups and concentrated using Amicon ultrafiltration tubes. Using NTA, size and concentration of EVs were measured (**Table 4**).

Table 4: **Characterization results of AMSC derived EVs by NTA.** EVs were collected from total 3 wells that contains 100.000 AMSCs each. Only medium sample was concentrated starvation medium that did not used for any cell treatment. SD: standard deviation.

Samples	Mean size [nm]	Mode [nm]	SD [nm]	Total concentration [particles/ml]
EVs	181	141	70	1.25E+10
Stimulated EVs	172	140	102	3.14E+10
EVs-antimiR-155	204	170	109	1.27E+10
Stimulated-antimiR-155 EVs	200	187	102	1.69E+10
Only medium	134	111	106	4.50E+07

Compared to the 50.000 AMSCs, seeding 100.000 AMSCs/ml doubled the total concertation of secreted EVs. While the concentration of EVs is relatively similar between stimulated and unstimulated groups, only stimulated EVs show very high concentrations. These results follow our cell counting data. When we counted the cells after collection of the medium, the stimulated EVs treated cells showed the highest concentration of cells. AMSCs create clumps when they detach from the surface. The reason only one group had higher cell numbers could be that for those wells, and cells might create some clumps during cell seeding. Moreover, the EVS's mean size was not affected by stimulations. Again, we see that the highest concentrated EV population was the same size as the exosomes (**Appendix A**).

4.4.5. PCR Results

There are different methods to load exosomes with nucleic acids. Passive loading includes the incubation of RNA with exosomes. Despite its easy application, RNAs generally end up sticking to the surface of the exosomes rather than diffusing inside. Another method is electroporation to induce transient pores on the exosome membrane that allow RNA transport. However, the cations released from metal electrode co-precipitate RNA, and the encapsulation efficiency of RNA is insignificant [104,105]. Thus, researchers also tried alternative methods to increase the encapsulation efficiency of RNAs into exosomes. MicroRNA encapsulated Lentiviral (LV) particles were used to transfect MSCs to obtain miRNA-rich exosomes [106,107]. Commercially available transfection reagents are another option that was shown to be effective. Shimbo et al. transfected MSCs with miR-143 mimic using Lipofectamine and observed that exosomes collected from transfected MSCs successfully suppress migration of cancer cells [108]. In our experimental design, we also used the transfection reagent HiPerFect to load interested antimiR-155 during the formation of EVs to treat inflammatory macrophages.

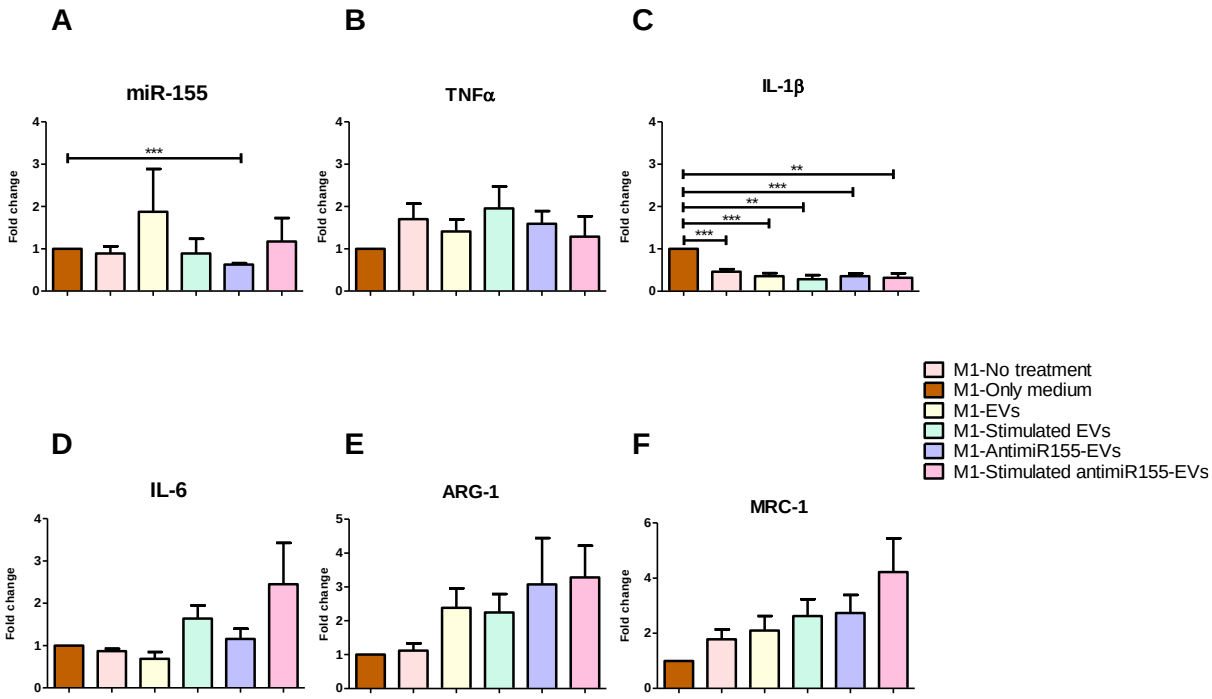

Figure 30: Gene expression levels after EV treatment of Raw macrophages. AMSCs starved with or without 20ng/ml TNF-α and 20ng/ml IF-γ stimulation for 48h. Additionally, starving AMSCs treated with 2µg/ml anti-miR-155 containing HiPerFect transfection reagent during starvation. Medium was collected and concentrated using Amicon ultrafiltration tubes at 2000g for 20 min. Raw cells were treated with concentrated EVs for 24h and stimulated 6h with 100ng/ml LPS and 20ng/ml IFN-γ for obtaining proinflammatory M1 macrophages. Only medium sample was concentrated starvation medium that did not used for any cell treatment. All genes normalized to GAPDH. Significance was determined with the unpaired t-test, CI 95%, *p<0.05, **p<0.01, ***, p<0.001.

We observed a significant reduction (1.5-fold) in miR-155 expression after transfecting antimiR-155 loaded EV treatment (in **Figure 30-A**). However, stimulated antimiR-155 loaded exosomes did not show the same effect. The reason could be that the residual stimuli cancel out the effect of antimiR-155 by increasing the expression of miR-155 as a pro-inflammatory response.

Even though we increased the concentration of collected EVs by seeding 100.000 AMSCs/ml instead of 50.000, we still did not observe any significant reduction in TNFα or IL-6 (from **Figure 30-B, D**). Surprisingly, despite a significant decrease in miR-155 expression after antimiR-155 loaded EV treatment, the reduction was not projected to IL-6 or TNFα expressions. When we used LNPs as a delivery vehicle for antimiR-155, we observed a 2-fold reduction in miR-155 expression (in **Figure 25**). However, with EVs, we only observed around a 1.5-fold change. Thus, the reason that we could not see any mitigation in pro-inflammatory response might be due to the insufficient repression of miR-155. Higher RNA concentrations might be necessary to transfect AMSCs.

In accordance with our first PCR results (**Figure 29-B**), IL-1β levels significantly reduced after the treatment with EVs (in **Figure 30-C**). On the other hand, it is also clear that there is no additional reduction brought by miR-155 transfection. Surprisingly, with IL-1β expression, only starvation medium negative control appears to have a pro-inflammatory effect. However, this result is unexpected and does not reflect reality because no other gene shows the same trend despite being obtained from the same samples. We assumed the reason for this induction in IL-1β expression after only medium treatment is the pipetting errors that occur during PCR.

As expected, higher ARG1 and MRC1 expressions were observed with higher EV concentration but still not pronounced (in **Figure 30-E, F**). It seems like EVs have the potential to stimulate the pro-inflammatory response, but we still could not find the potent concentration range to have a significant induction. Nevertheless, antimiR-155 transfection does not seem to affect the expression of M2 marker expression.

In literature, researchers isolated exosomes from EVs using different methods such as ultracentrifugation [109] or Exoquick™ precipitation [46] and treated different cells with this isolated exosome instead of EVs. However, during these experiments, we did not isolate exosomes but used EVs. To see the effect of exosomes solely, we should isolate them from collected EVs for future experiments. In addition, we do not know the purity of isolated AMSCs. For the following experiments, AMSCs can be stained by MSC markers such as CD90 and CD105 [110] and sorted using FACS to obtain a 100% pure MSC population.

5. Conclusion

The pathophysiology of NASH has been described in a multi-hit scenario and is characterized by inflammation [6]. There are still no treatments and no drugs that have been licensed even though NASH is the most prevalent liver disease [16]. Some anti-inflammatory medications have been used to target the inflammatory axis of NASH; however, finding alternative methods is necessary due to the adverse immune responses. Since altered miRNA profiles were observed in NASH, researchers' focus has recently shifted to RNAs [19]. MiRNAs are small non-coding RNAs which have a length of 19 to 25 nucleotides and can control post-transcriptional gene expression by attaching to the 3' UTRs of target mRNAs.[20] MiRNAs are responsible for fine-tuning pathological and physiological processes in the liver. MiRNAs are well-known for being essential controllers of innate and adaptive immunity [30]. Therefore, their expression is under tight and dynamic control. Among different miRNAs, miR-155 is described as a central regulator of inflammation and found to be overexpressed in NASH [36,39,50,51]. Throughout this study, our primary goal was to reduce the miR-155 overexpression in inflammatory macrophages by delivering a miRNA therapeutic, antimiR-155, that silences miR-155. Apart from miR-155, the expression of pro-inflammatory cytokines IL-6 and TNF-α associated with miR-155 were also targeted. As a nanocarrier, HiPerFect transfection reagent, lipid nanoparticles, and adipose mesenchymal stem cell-derived extracellular vesicles were used to find an optimum nanocarrier system for antimiR-155.

After observing the overexpression of miR-155 in M1 macrophages, antimiR-155 was delivered first using HiPerFect transfection reagent. After 24h, a significant reduction in miR-155 expression along with reduced levels of pro-inflammatory cytokines TNFα and IL-6 were observed. Despite the efficient transfection, the cell viability assay showed reduced metabolic activity in macrophages. Therefore, as a next step, antimiR-155 was delivered using LNPs to overcome the toxicity issue of charged lipids in HiPerFect solution. In LNP formulation, instead of charged lipids, we used ionizable lipid MC3, which is not charged at neutral pH but positively charged in acidic pH to stimulate the endosomal escape. First, we analyzed the uptake behavior of LNPs by different liver cells and as a result, macrophages and endothelial cells showed the highest uptake. Alamar Blue assay results showed that 10mM LNP formulation did not have any negative effect on cell viability. Thus, we concluded that 10mM MC3 containing LNPs were a promising nanocarrier for the treatment of liver inflammation through targeting macrophages. After optimizing the lipid concentration in LNP formulations, antimiR-155 was encapsulated into 10mM LNPs by using a microfluidic device. PCR and ELISA results showed significant downregulation of miR-155 along with TNFα and IL-6. Thus, using LNPs as a nanocarrier, we obtained the same transfection efficiency as HiPerFect together with enhanced viability. Therefore, LNPs found as a better alternative than commercially available transfection reagents, and they have a remarkable potential to be used in the treatment of NASH. The successful *in vitro* transfection of LNPs is opening the ways for the future *in vivo* studies.

In the last section, we analyzed the RNA-carrying potential of extracellular vehicles (EVs). EVs were isolated from AMSCs because AMSCs have the innate capacity to suppress inflammatory cytokines and increase anti-inflammatory ones. Unfortunately, a reduction in TNFα or IL-6 could not be observed even though the different concentrations of EVs were used. Moreover, we were able to demonstrate a significant reduction in IL-1β expression along with an enhanced level of M2 markers, including ARG-

1 and MRC-1. However, delivering antimiR-155 did not contribute to the innate capacity of EVs in ameliorating inflammation despite the significant reduction in miR-155 expression. This might be due to the insufficient concentration. To draw a conclusion on the capacity of AMSC-derived EVs, more experiment needs to be carried out.

6. Future Perspective

The *in-vitro* results from this study establish a promising anti-inflammatory effect for antimiR-155 when transfected using MC3 containing LNPs. MicroRNA-155 is overexpressed in NASH and HCC and exacerbates the formation of the disease. Finding an optimum delivery vehicle for antimiR-155 paves the way for new therapies for liver diseases. However, it is known that MC3 might accumulate in the body after multiple injections due to its slow biodegradability. Primary ester modifications of MC3 (L319) showed better tolerability of LNPs by enabling fast metabolism in the liver [70,111]. In addition, COVID-19 vaccines use biodegradable lipids SM-102 and ALC-0315 that have better *in vivo* delivery efficacy and pharmacokinetics than MC3 [70]. Therefore, as the next step of LNP experiments, modified lipids that have faster biodegradability can be used to enable multiple injections. Using fluorescently labelled lipid components might help with evaluating the biodegradability of the LNPs. Besides improving LNP formulation, combinational therapies might also increase the effectivity of antimiR-155. Chen et al. delivered 1,25-dihydroxy vitamin D [1,25(OH)2D3], the active metabolite of vitamin D, to macrophages and results showed attenuated inflammation upon LPS exposure mediated by downregulated miR-155. Together with miR-155, TNFα and IL-6 levels were also suppressed [112]. Thus, incorporating 1,25(OH)2D3 together with antimiR-155 might lead to better suppression of miR-155, TNFα, and IL-6.

The potential of MSC-derived exosomes paves the way for cell-free regenerative medicine. Using MSC-derived exosomes instead of MSCs diminishes the safety concern and limitations associated with cell transplantation. Among the advantages of MSC-derived exosomes, crossing the blood-brain barrier, low immunogenicity, and non-oncogenicity can be mentioned. Exosomes can be extracted from the patient's own body fluids or cell culture. These autologous exosomes provide potential as individualized drug delivery systems [75]. As a scope of this project, we analyzed the anti-inflammatory potential of AMSC-derived EVs. However, we were not able to isolate exosomes solely. Therefore, as the next step, exosomes should be isolated from EVs by using ultracentrifugation. This way, the potent exosome concentration can be determined with more sensitivity. In addition, through ultracentrifugation, we might remove the residual of TNFα and IF-γ stimulation that caused higher pro-inflammatory response. Concentrated exosomes might also be used to identify the miRNA profile inside the AMSC-derived exosomes. One of the biggest challenges of exosomes as nanocarriers is loading RNAs. Therefore, we chose to transfect MSCs instead of exosomes. Even though we were successfully incorporate antimiR-155 into the AMSCs-derived EVs, the concentration of RNA was not high enough to mitigate the pro-inflammatory response. Thus, different concentrations of antimiR-155 should also be tested in the future.

7. Future Recommendations

In this research, we delivered antimiR-155 to pro-inflammatory macrophages and observed the downregulation of miR-155 along with pro-inflammatory cytokines. In addition, it is known that miR-155 is also overexpressed in hepatocytes during inflammation. Therefore, delivering antimiR-155 to hepatocytes and examining the miR-155 expression is recommended. MiR-155 is overexpressed in HCC cells as well. Therefore, we should also deliver antimiR-155 to mouse HCC cells.

For LNP formulations, we only produced neutral particles. Using DSPG instead of DSPC will make negatively charged particles more specific to liver macrophages [93]. Thus, before trying our LNP formulation *in vivo*, I would suggest comparing the potential of neutral and negatively charged particles to target macrophages *in vitro*. Whichever formulation outcompetes, *in vivo* experiments can carry out with it. I advise adding one more formulation that includes the encapsulation of miR-146 together with antimiR-155. Adding another RNA might change the parameters of the LNP formulation. Hence, another optimization process is necessary for dual delivery.

To improve the AMSCs isolation step, I recommend first staining them with MSC-specific markers and checking their purity. The second step might be sorting the stained cells to create a pure AMSCs population and culture them. After creating the mere population, we can produce EVs from them. The next step should be increasing exosome concentration until we observe a reduction in TNFα expression. We can do this by ultracentrifugation, which will also clear the pro-inflammatory stimuli from the starvation medium. After isolating exosomes from EVs, exosome surface marker CD63 can be measured using the western blot method to be sure the exosomes are isolated successfully. Lastly, I would suggest transfecting AMSCs with different antimiR-155 concentrations because even though we could deliver antimiR-155 to macrophages, it was not sufficient to mitigate the pro-inflammatory response.

8. References

[1] Michelotti GA, Machado M v., Diehl AM. NAFLD, NASH and liver cancer. Nat Rev Gastroenterol Hepatol 2013;10:656–65. https://doi.org/10.1038/nrgastro.2013.183.

[2] Marchesini G, Day CP, Dufour JF, Canbay A, Nobili V, Ratziu V, et al. EASL-EASD-EASO Clinical Practice Guidelines for the Management of Non-Alcoholic Fatty Liver Disease. Obes Facts 2016;9:65–90. https://doi.org/10.1159/000443344.

[3] Le MH, Yeo YH, Li X, Li J, Zou B, Wu Y, et al. 2019 Global NAFLD Prevalence: A Systematic Review and Meta-analysis. Clinical Gastroenterology and Hepatology 2022. https://doi.org/10.1016/j.cgh.2021.12.002.

[4] Marjot T, Moolla A, Cobbold JF, Hodson L, Tomlinson JW. Nonalcoholic Fatty Liver Disease in Adults: Current Concepts in Etiology, Outcomes, and Management. Endocr Rev 2020;41:66–117. https://doi.org/10.1210/ENDREV/BNZ009.

[5] Chalasani N, Younossi Z, Lavine JE, Diehl AM, Brunt EM, Cusi K, et al. The diagnosis and management of non-alcoholic fatty liver disease: Practice Guideline by the American Association for the Study of Liver Diseases, American College of Gastroenterology, and the American Gastroenterological Association. Hepatology 2012;55:2005–23. https://doi.org/10.1002/HEP.25762.

[6] Manne V, Handa P, Kowdley K v. Pathophysiology of Nonalcoholic Fatty Liver Disease/Nonalcoholic Steatohepatitis. Clin Liver Dis 2018;22:23–37. https://doi.org/10.1016/j.cld.2017.08.007.

[7] Sheka AC, Adeyi O, Thompson J, Hameed B, Crawford PA, Ikramuddin S. Nonalcoholic Steatohepatitis: A Review. JAMA - Journal of the American Medical Association 2020;323:1175–83. https://doi.org/10.1001/jama.2020.2298.

[8] Fingas CD, Best J, Sowa JP, Canbay A. Epidemiology of nonalcoholic steatohepatitis and hepatocellular carcinoma. Clin Liver Dis (Hoboken) 2016;8:119–22. https://doi.org/10.1002/cld.585.

[9] Puengel T, Liu H, Guillot A, Heymann F, Tacke F, Peiseler M. Nuclear Receptors Linking Metabolism, Inflammation, and Fibrosis in Nonalcoholic Fatty Liver Disease. Int J Mol Sci 2022;23. https://doi.org/10.3390/ijms23052668.

[10] Schwabe RF, Uchinami H, Qian T, Bennett BL, Lemasters JJ, Brenner DA. Differential requirement for c-Jun NH2-terminal kinase in TNFalpha- and Fas-mediated apoptosis in hepatocytes. The FASEB Journal : Official Publication of the Federation of American Societies for Experimental Biology 2004;18:720–2. https://doi.org/10.1096/FJ.03-0771FJE.

[11] Wan X, Xu C, Yu C, Li Y. Role of NLRP3 Inflammasome in the Progression of NAFLD to NASH. Can J Gastroenterol Hepatol 2016;2016. https://doi.org/10.1155/2016/6489012.

[12] Mirea A-M, Tack CJ, Chavakis T, Joosten LAB, Toonen EJM. IL-1 family cytokine pathways underlying NAFLD: towards new treatment strategies n.d. https://doi.org/10.1016/j.molmed.2018.03.005.

[13] Bocsan IC, Milaciu MV, Pop RM, Vesa SC, Ciumarnean L, Matei DM, et al. Cytokines Genotype-Phenotype Correlation in Nonalcoholic Steatohepatitis. Oxid Med Cell Longev 2017;2017. https://doi.org/10.1155/2017/4297206.

[14] Seki E, Schwabe RF. Hepatic inflammation and fibrosis: Functional links and key pathways. Hepatology 2015;61:1066–79. https://doi.org/10.1002/HEP.27332.

[15] Brandl K, Schnabl B. The intestinal microbiota and NASH. Curr Opin Gastroenterol 2017;33:128. https://doi.org/10.1097/MOG.0000000000000349.

[16] Lazaridis N, Tsochatzis E. Current and future treatment options in non-alcoholic steatohepatitis (NASH). Https://DoiOrg/101080/1747412420171293523 2017;11:357–69. https://doi.org/10.1080/17474124.2017.1293523.

[17] Takaki A, Kawai D, Yamamoto K. Molecular mechanisms and new treatment strategies for non-alcoholic steatohepatitis (NASH). Int J Mol Sci 2014;15:7352–79. https://doi.org/10.3390/ijms15057352.

[18] Lou G, Chen Z, Zheng M, Liu Y. Mesenchymal stem cell-derived exosomes as a new therapeutic strategy for liver diseases. Exp Mol Med 2017;49:e346. https://doi.org/10.1038/EMM.2017.63.

[19] Szabo G, Csak T. Role of MicroRNAs in NAFLD/NASH. Dig Dis Sci 2016;61:1314–24. https://doi.org/10.1007/s10620-015-4002-4.

[20] Hammond SM. An overview of microRNAs. Adv Drug Deliv Rev 2015;87:3–14. https://doi.org/10.1016/J.ADDR.2015.05.001.

[21] Mah S and BC and HK and KF. miRNA*: A Passenger Stranded in RNA-Induced Silencing Complex? 2010. https://doi.org/10.1615/CritRevEukarGeneExpr.v20.i2.40.

[22] Ha M, Kim VN. Regulation of microRNA biogenesis. Nat Rev Mol Cell Biol 2014;15:509–24. https://doi.org/10.1038/nrm3838.

[23] Schueller F, Roy S, Vucur M, Trautwein C, Luedde T, Roderburg C. The Role of miRNAs in the Pathophysiology of Liver Diseases and Toxicity. International Journal of Molecular Sciences 2018, Vol 19, Page 261 2018;19:261. https://doi.org/10.3390/IJMS19010261.

[24] Wang X, He Y, Mackowiak B, Gao B. MicroRNAs as regulators, biomarkers and therapeutic targets in liver diseases. Gut 2021;70:784–95. https://doi.org/10.1136/gutjnl-2020-322526.

[25] Hammond SM. An overview of microRNAs. Adv Drug Deliv Rev 2015;87:3. https://doi.org/10.1016/J.ADDR.2015.05.001.

[26] Torres J-L, Novo-Veleiro I, Manzanedo L, Alvela-Suárez L, Macías R, Laso F-J, et al. Role of microRNAs in alcohol-induced liver disorders and non-alcoholic fatty liver disease. World J Gastroenterol 2018;24:4104. https://doi.org/10.3748/WJG.V24.I36.4104.

[27] Y H, C H, SP Z, X S, XR L, J L. The potential of microRNAs in liver fibrosis. Cell Signal 2012;24:2268–72. https://doi.org/10.1016/J.CELLSIG.2012.07.023.

[28] Tilg H, Moschen AR. Evolution of inflammation in nonalcoholic fatty liver disease: The multiple parallel hits hypothesis. Hepatology 2010;52:1836–46. https://doi.org/10.1002/hep.24001.

[29] Szabo G, Csak T. Role of MicroRNAs in NAFLD/NASH. Dig Dis Sci 2016;61:1314–24. https://doi.org/10.1007/s10620-015-4002-4.

[30] Szabo G, Bala S. MicroRNAs in liver disease. Nat Rev Gastroenterol Hepatol 2013;10:542–52. https://doi.org/10.1038/nrgastro.2013.87.

[31] Szabo M. Emerging role of microRNAs in liver diseases. World J Gastroenterol 2009;15:5633–40. https://doi.org/10.3748/wjg.15.5633.

[32] Curtale G, Rubino M, Locati M. MicroRNAs as molecular switches in macrophage activation. Front Immunol 2019;10:799. https://doi.org/10.3389/FIMMU.2019.00799/BIBTEX.

[33] Boldin MP, Taganov KD, Rao DS, Yang L, Zhao JL, Kalwani M, et al. miR-146a is a significant brake on autoimmunity, myeloproliferation, and cancer in mice. Journal of Experimental Medicine 2011;208:1189–201. https://doi.org/10.1084/jem.20101823.

[34] Wen J, Friedman JR. miR-122 regulates hepatic lipid metabolism and tumor suppression. J Clin Invest 2012;122:2773. https://doi.org/10.1172/JCI63966.

[35] Roy S, Benz F, Luedde T, Roderburg C. The role of miRNAs in the regulation of inflammatory processes during hepatofibrogenesis. Hepatobiliary Surg Nutr 2015;4:24. https://doi.org/10.3978/J.ISSN.2304-3881.2015.01.05.

[36] Gulei D, Raduly L, Broseghini E, Ferracin M, Berindan-Neagoe I. The extensive role of miR-155 in malignant and non-malignant diseases. Mol Aspects Med 2019;70:33–56. https://doi.org/10.1016/j.mam.2019.09.004.

[37] Mashima R. Physiological roles of miR-155. Immunology 2015;145:323. https://doi.org/10.1111/IMM.12468.

[38] Li Y, Kowdley K v. MicroRNAs in Common Human Diseases. Genomics Proteomics Bioinformatics 2012;10:246–53. https://doi.org/10.1016/J.GPB.2012.07.005.

[39] Wang B, Majumder S, Nuovo G, Kutay H, Volinia S, Patel T, et al. Role of miR-155 at early stages of hepatocarcinogenesis induced by choline-deficient and amino acid defined diet in C57BL/6 mice. Hepatology 2009;50:1152. https://doi.org/10.1002/HEP.23100.

[40] Tang B, Lei B, Qi G, Liang X, Tang F, Yuan S, et al. MicroRNA-155-3p promotes hepatocellular carcinoma formation by suppressing FBXW7 expression. Journal of Experimental and Clinical Cancer Research 2016;35:1–12. https://doi.org/10.1186/S13046-016-0371-6/FIGURES/11.

[41] Zhang Y, Wei W, Cheng N, Wang K, Li B, Jiang X, et al. Hepatitis C virus-induced up-regulation of microRNA-155 promotes hepatocarcinogenesis by activating Wnt signaling. Hepatology 2012;56:1631–40. https://doi.org/10.1002/HEP.25849.

[42] Blaya D, Coll M, Rodrigo-Torres D, Vila-Casadesús M, Altamirano J, Llopis M, et al. Integrative microRNA profiling in alcoholic hepatitis reveals a role for microRNA-182 in liver injury and inflammation. Gut 2016;65:1535–45. https://doi.org/10.1136/gutjnl-2015-311314.

[43] Blaya D, Aguilar-Bravo B, Hao F, Casacuberta-Serra S, Coll M, Perea L, et al. Expression of microRNA-155 in inflammatory cells modulates liver injury. Hepatology 2018;68:691. https://doi.org/10.1002/HEP.29833.

[44] Fu X, Wen H, Jing L, Yang Y, Wang W, Liang X, et al. MicroRNA-155-5p promotes hepatocellular carcinoma progression by suppressing PTEN through the PI3K/Akt pathway. Cancer Sci 2017;108:620. https://doi.org/10.1111/CAS.13177.

[45] Alivernini S, Gremese E, McSharry C, Tolusso B, Ferraccioli G, McInnes IB, et al. MicroRNA-155-at the critical interface of innate and adaptive immunity in arthritis. Front Immunol 2018;8:1932. https://doi.org/10.3389/FIMMU.2017.01932/BIBTEX.

[46] Momen-Heravi F, Bala S, Bukong T, Szabo G. Exosome-mediated delivery of functionally active miRNA-155 inhibitor to macrophages. Nanomedicine 2014;10:1517. https://doi.org/10.1016/J.NANO.2014.03.014.

[47] Cai X, Yin Y, Li N, Zhu D, Zhang J, Zhang CY, et al. Re-polarization of tumor-associated macrophages to pro-inflammatory M1 macrophages by microRNA-155. J Mol Cell Biol 2012;4:341–3. https://doi.org/10.1093/JMCB/MJS044.

[48] Jablonski KA, Gaudet AD, Amici SA, Popovich PG, Guerau-de-Arellano M. Control of the Inflammatory Macrophage Transcriptional Signature by miR-155. PLoS One 2016;11. https://doi.org/10.1371/JOURNAL.PONE.0159724.

[49] Worm J, Stenvang J, Petri A, Frederiksen KS, Obad S, Elmén J, et al. Silencing of microRNA-155 in mice during acute inflammatory response leads to derepression of c/ebp Beta and down-regulation of G-CSF. Nucleic Acids Res 2009;37:5784. https://doi.org/10.1093/NAR/GKP577.

[50] Miller AM, Gilchrist DS, Nijjar J, Araldi E, Ramirez CM, Lavery CA, et al. MiR-155 Has a Protective Role in the Development of Non-Alcoholic Hepatosteatosis in Mice. PLoS One 2013;8:72324. https://doi.org/10.1371/JOURNAL.PONE.0072324.

[51] Csak T, Bala S, Lippai D, Kodys K, Catalano D, Iracheta-Vellve A, et al. MicroRNA-155 deficiency attenuates liver steatosis and fibrosis without reducing inflammation in a mouse model of steatohepatitis. PLoS One 2015;10. https://doi.org/10.1371/journal.pone.0129251.

[52] Tili E, Michaille J-J, Cimino A, Costinean S, Dumitru CD, Adair B, et al. Modulation of miR-155 and miR-125b levels following lipopolysaccharide/TNF-alpha stimulation and their possible roles in regulating the response to endotoxin shock. J Immunol 2007;179:5082–9. https://doi.org/10.4049/JIMMUNOL.179.8.5082.

[53] Bala S, Marcos M, Kodys K, Csak T, Catalano D, Mandrekar P, et al. Up-regulation of microRNA-155 in macrophages contributes to increased tumor necrosis factor {alpha} (TNF{alpha}) production via increased mRNA half-life in alcoholic liver disease. J Biol Chem 2011;286:1436–44. https://doi.org/10.1074/JBC.M110.145870.

[54] Jablonski KA, Amici SA, Webb LM, Ruiz-Rosado JDD, Popovich PG, Partida-Sanchez S, et al. Novel Markers to Delineate Murine M1 and M2 Macrophages. PLoS One 2015;10:e0145342. https://doi.org/10.1371/JOURNAL.PONE.0145342.

[55] Bajan S, Hutvagner G. RNA-Based Therapeutics: From Antisense Oligonucleotides to miRNAs. Cells 2020;9. https://doi.org/10.3390/cells9010137.

[56] Abdallah F, Pichon C. MicroRNAs in Skin Biology: Biogenesis, Regulations and Functions in Homeostasis and Diseases. Immunome Res 2019;15. https://doi.org/10.35248/1745-7580.19.15.169.

[57] Cheng X, Lee RJ. The role of helper lipids in lipid nanoparticles (LNPs) designed for oligonucleotide delivery. Adv Drug Deliv Rev 2016;99:129–37. https://doi.org/10.1016/j.addr.2016.01.022.

[58] Thomson DW, Dinger ME. Endogenous microRNA sponges: Evidence and controversy. Nat Rev Genet 2016;17:272–83. https://doi.org/10.1038/nrg.2016.20.

[59] Deleavey GF, Watts JK, Damha MJ. Chemical modification of siRNA. Curr Protoc Nucleic Acid Chem 2009. https://doi.org/10.1002/0471142700.nc1603s39.

[60] Krützfeldt J, Rajewsky N, Braich R, Rajeev KG, Tuschl T, Manoharan M, et al. Silencing of microRNAs in vivo with "antagomirs." Nature 2005;438:685–9. https://doi.org/10.1038/nature04303.

[61] Davis S, Lollo B, Freier S, Esau C. Improved targeting of miRNA with antisense oligonucleotides. Nucleic Acids Res 2006;34:2294–304. https://doi.org/10.1093/nar/gkl183.

[62] Ørom UA, Kauppinen S, Lund AH. LNA-modified oligonucleotides mediate specific inhibition of microRNA function. Gene 2006;372:137–41. https://doi.org/10.1016/j.gene.2005.12.031.

[63] Bouchie A. First microRNA mimic enters clinic. Nat Biotechnol 2013;31:577. https://doi.org/10.1038/NBT0713-577.

[64] Su Q, Kumar V, Sud N, Mahato RI. Role of MicroRNAs in the Pathogenesis and Treatment of Progressive Liver Injury in NAFLD and Liver Fibrosis. 2018.

[65] Witten L, Slack FJ. miR-155 as a novel clinical target for hematological malignancies. Carcinogenesis 2020;41:2–7. https://doi.org/10.1093/CARCIN/BGZ183.

[66] Zatsepin TS, Kotelevtsev Y v., Koteliansky V. Lipid nanoparticles for targeted siRNA delivery - Going from bench to bedside. Int J Nanomedicine 2016;11:3077–86. https://doi.org/10.2147/IJN.S106625.

[67] Tam YYC, Chen S, Cullis PR. Advances in Lipid Nanoparticles for siRNA Delivery. Pharmaceutics 2013;5:498. https://doi.org/10.3390/PHARMACEUTICS5030498.

[68] Wan C, Allen TM, Cullis PR. Lipid nanoparticle delivery systems for siRNA-based therapeutics. Drug Deliv Transl Res 2014;4:74–83. https://doi.org/10.1007/s13346-013-0161-z.

[69] Akinc A, Maier MA, Manoharan M, Fitzgerald K, Jayaraman M, Barros S, et al. The Onpattro story and the clinical translation of nanomedicines containing nucleic acid-based drugs. Nature Nanotechnology 2019 14:12 2019;14:1084–7. https://doi.org/10.1038/s41565-019-0591-y.

[70] Hou X, Zaks T, Langer R, Dong Y. Lipid nanoparticles for mRNA delivery. Nat Rev Mater 2021;6:1078–94. https://doi.org/10.1038/s41578-021-00358-0.

[71] Bala S, Csak T, Saha B, Zatsiorsky J, Kodys K, Catalano D, et al. The pro-inflammatory effects of miR-155 promote liver fibrosis and alcohol-induced steatohepatitis. J Hepatol 2016;64:1378. https://doi.org/10.1016/J.JHEP.2016.01.035.

[72] Teng C, Lin C, Huang F, Xing X, Chen S, Ye L, et al. Intracellular codelivery of anti-inflammatory drug and anti-miR 155 to treat inflammatory disease. Acta Pharm Sin B 2020;10:1521–33. https://doi.org/10.1016/j.apsb.2020.06.005.

[73] Zhang M, Zhou X, Wang B, Yung BC, Lee LJ, Ghoshal K, et al. Lactosylated gramicidin-based lipid nanoparticles (Lac-GLN) for targeted delivery of anti-miR-155 to hepatocellular carcinoma. Journal of Controlled Release 2013;168:251–61. https://doi.org/10.1016/j.jconrel.2013.03.020.

[74] el Andaloussi S, Mäger I, Breakefield XO, Wood MJA. Extracellular vesicles: Biology and emerging therapeutic opportunities. Nat Rev Drug Discov 2013;12:347–57. https://doi.org/10.1038/nrd3978.

[75] Arabpour M, Saghazadeh A, Rezaei N. Anti-inflammatory and M2 macrophage polarization-promoting effect of mesenchymal stem cell-derived exosomes. Int Immunopharmacol 2021;97. https://doi.org/10.1016/j.intimp.2021.107823.

[76] Hidalgo-Garcia L, Galvez J, Rodriguez-Cabezas ME, Anderson PO. Can a conversation between mesenchymal stromal cells and macrophages solve the crisis in the inflamed intestine? Front Pharmacol 2018;9:179. https://doi.org/10.3389/FPHAR.2018.00179/BIBTEX.

[77] Harrell CR, Jovicic N, Djonov V, Arsenijevic N, Volarevic V. Mesenchymal Stem Cell-Derived Exosomes and Other Extracellular Vesicles as New Remedies in the Therapy of Inflammatory Diseases. Cells 2019;8. https://doi.org/10.3390/CELLS8121605.

[78] Liu Y, Lou G, Li A, Zhang T, Qi J, Ye D, et al. AMSC-derived exosomes alleviate lipopolysaccharide/d-galactosamine-induced acute liver failure by miR-17-mediated reduction of TXNIP/NLRP3 inflammasome activation in macrophages. EBioMedicine 2018;36:140. https://doi.org/10.1016/J.EBIOM.2018.08.054.

[79] Zhao H, Shang Q, Pan Z, Bai Y, Li Z, Zhang H, et al. Exosomes From Adipose-Derived Stem Cells Attenuate Adipose Inflammation and Obesity Through Polarizing M2 Macrophages and Beiging in White Adipose Tissue. Diabetes 2018;67:235–47. https://doi.org/10.2337/DB17-0356.

[80] Domenis R, Cifù A, Quaglia S, Pistis C, Moretti M, Vicario A, et al. Pro inflammatory stimuli enhance the immunosuppressive functions of adipose mesenchymal stem cells-derived exosomes. Scientific Reports 2018 8:1 2018;8:1–11. https://doi.org/10.1038/s41598-018-31707-9.

[81] Chen Y-T, Sun C-K, Lin Y-C, Chang L-T, Chen Y-L, Tsai T-H, et al. Adipose-Derived Mesenchymal Stem Cell Protects Kidneys against Ischemia-Reperfusion Injury through Suppressing Oxidative Stress and Inflammatory Reaction. J Transl Med 2011;9:51. https://doi.org/10.1186/1479-5876-9-51.

[82] Jankowski M, Dompe C, Sibiak R, Wąsiatycz G, Mozdziak P, Jaśkowski JM, et al. In Vitro Cultures of Adipose-Derived Stem Cells: An Overview of Methods, Molecular Analyses, and Clinical Applications. Cells 2020, Vol 9, Page 1783 2020;9:1783. https://doi.org/10.3390/CELLS9081783.

[83] Chen C, Ridzon DA, Broomer AJ, Zhou Z, Lee DH, Nguyen JT, et al. Real-time quantification of microRNAs by stem–loop RT–PCR. Nucleic Acids Res 2005;33:e179–e179. https://doi.org/10.1093/NAR/GNI178.

[84] Carralot J-P, Kim T-K, Lenseigne B, Boese AS, Sommer P, Genovesio A, et al. Automated High-Throughput siRNA Transfection in Raw 264.7 Macrophages: A Case Study for Optimization Procedure 2009. https://doi.org/10.1177/1087057108328762.

[85] Arteta MY, Kjellman T, Bartesaghi S, Wallin S, Wu X, Kvist AJ, et al. Successful reprogramming of cellular protein production through mRNA delivered by functionalized lipid nanoparticles. Proc Natl Acad Sci U S A 2018;115:E3351–60. https://doi.org/10.1073/pnas.1720542115.

[86] Martinez-Nunez RT, Louafi F, Sanchez-Elsner T. The Interleukin 13 (IL-13) Pathway in Human Macrophages Is Modulated by MicroRNA-155 via Direct Targeting of Interleukin 13 Receptor α1 (IL13Rα1). J Biol Chem 2011;286:1786. https://doi.org/10.1074/JBC.M110.169367.

[87] Racanelli V, Rehermann B. The liver as an immunological organ. Hepatology 2006;43:S54–62. https://doi.org/10.1002/HEP.21060.

[88] Knolle PA, Gerken G. Local control of the immune response in the liver. Immunol Rev 2000;174:21–34. https://doi.org/10.1034/J.1600-0528.2002.017408.X.

[89] Li D, Friedman SL. Liver fibrogenesis and the role of hepatic stellate cells: New insights and prospects for therapy. Journal of Gastroenterology and Hepatology (Australia) 1999;14:618–33. https://doi.org/10.1046/J.1440-1746.1999.01928.X.

[90] Semple SC, Chonn A, Cullis PR. Interactions of liposomes and lipid-based carrier systems with blood proteins: Relation to clearance behaviour in vivo. vol. 32. 1998.

[91] Witzigmann D, Kulkarni JA, Leung J, Chen S, Cullis PR, van der Meel R. Lipid nanoparticle technology for therapeutic gene regulation in the liver. Adv Drug Deliv Rev 2020;159:344–63. https://doi.org/10.1016/j.addr.2020.06.026.

[92] Sago CD, Krupczak BR, Lokugamage MP, Gan Z, Dahlman JE. Cell Subtypes Within the Liver Microenvironment Differentially Interact with Lipid Nanoparticles n.d. https://doi.org/10.1007/s12195-019-00573-4.

[93] Pattipeiluhu R, Arias-Alpizar G, Basha G, Chan KYT, Bussmann J, Sharp TH, et al. Anionic Lipid Nanoparticles Preferentially Deliver mRNA to the Hepatic Reticuloendothelial System. Advanced Materials 2022:2201095. https://doi.org/10.1002/ADMA.202201095.

[94] Parameswaran N, Patial S. Tumor Necrosis Factor-α Signaling in Macrophages 2010.

[95] Sørensen KK, Simon-Santamaria J, McCuskey RS, Smedsrød B. Liver sinusoidal endothelial cells. Compr Physiol 2015;5:1751–74. https://doi.org/10.1002/cphy.c140078.

[96] Rafique A, Etzerodt A, Graversen JH, Moestrup SK, Dagnæs-Hansen F, Møller HJ. Targeted lipid nanoparticle delivery of calcitriol to human monocyte-derived macrophages in vitro and in vivo: Investigation of the anti-inflammatory effects of calcitriol. Int J Nanomedicine 2019;14:2829–46. https://doi.org/10.2147/IJN.S192113.

[97] George Joju, Abel Peter. Pentoxifylline. 2008. https://doi.org/https://doi.org/10.1016/B978-008055232-3.63921-2.

[98] Li K, Ching D, Luk FS, Raffai RL. Apolipoprotein e Enhances MicroRNA-146a in Monocytes and Macrophages to Suppress Nuclear Factor-κB-Driven Inflammation and Atherosclerosis. Circ Res 2015;117:e1–11. https://doi.org/10.1161/CIRCRESAHA.117.305844/FORMAT/EPUB.

[99] Iyer SS, Rojas M. Anti-inflammatory effects of mesenchymal stem cells: novel concept for future therapies. Http://DxDoiOrg/101517/1471259885569 2008;8:569–81. https://doi.org/10.1517/14712598.8.5.569.

[100] Volarevic V, Markovic BS, Gazdic M, Volarevic A, Jovicic N, Arsenijevic N, et al. Ethical and safety issues of stem cell-based therapy. Int J Med Sci 2018;15:36–45. https://doi.org/10.7150/ijms.21666.

[101] Wang J, Xia J, Huang R, Hu Y, Fan J, Shu Q, et al. Mesenchymal stem cell-derived extracellular vesicles alter disease outcomes via endorsement of macrophage polarization. Stem Cell Research & Therapy 2020 11:1 2020;11:1–12. https://doi.org/10.1186/S13287-020-01937-8.

[102] Nahid MA, Satoh M, Chan EKL. E-Mail Interleukin 1β-Responsive MicroRNA-146a Is Critical for the Cytokine-Induced Tolerance and Cross-Tolerance to Toll-Like Receptor Ligands 2015. https://doi.org/10.1159/000371517.

[103] Li H, Jiang T, Li MQ, Zheng XL, Zhao GJ. Transcriptional regulation of macrophages polarization by microRNAs. Front Immunol 2018;9:1175. https://doi.org/10.3389/FIMMU.2018.01175/BIBTEX.

[104] Rankin-Turner S, Vader P, O'Driscoll L, Giebel B, Heaney LM, Davies OG. A call for the standardised reporting of factors affecting the exogenous loading of extracellular vesicles with therapeutic cargos. Adv Drug Deliv Rev 2021;173:479–91. https://doi.org/10.1016/J.ADDR.2021.04.012.

[105] Vader P, Kooijmans SA, Stremersch S, Raemdonck K. New considerations in the preparation of nucleic acid-loaded extracellular vesicles. Ther Deliv 2014;5:105–7. https://doi.org/10.4155/tde.13.142.

[106] Zhang K, Dong C, Chen M, Yang T, Wang X, Gao Y, et al. Extracellular vesicle-mediated delivery of miR-101 inhibits lung metastasis in osteosarcoma. Theranostics 2020;10:411. https://doi.org/10.7150/THNO.33482.

[107] Lou G, Yang Y, Liu F, Ye B, Chen Z, Zheng M, et al. MiR-122 modification enhances the therapeutic efficacy of adipose tissue-derived mesenchymal stem cells against liver fibrosis n.d. https://doi.org/10.1111/jcmm.13208.

[108] Shimbo K, Miyaki S, Ishitobi H, Kato Y, Kubo T, Shimose S, et al. Exosome-formed synthetic microRNA-143 is transferred to osteosarcoma cells and inhibits their migration. Biochem Biophys Res Commun 2014;445:381–7. https://doi.org/10.1016/j.bbrc.2014.02.007.

[109] Choi EW, Seo MK, Woo EY, Kim SH, Park EJ, Kim S. Exosomes from human adipose-derived stem cells promote proliferation and migration of skin fibroblasts. Exp Dermatol 2018;27:1170–2. https://doi.org/10.1111/EXD.13451.

[110] Shang Q, Bai Y, Wang G, Song Q, Guo C, Zhang L, et al. Delivery of Adipose-Derived Stem Cells Attenuates Adipose Tissue Inflammation and Insulin Resistance in Obese Mice Through Remodeling Macrophage Phenotypes. Stem Cells Dev 2015;24:2052–64. https://doi.org/10.1089/SCD.2014.0557/SUPPL_FILE/SUPP_FIG7.PDF.

[111] Maier MA, Jayaraman M, Matsuda S, Liu J, Barros S, Querbes W, et al. Biodegradable Lipids Enabling Rapidly Eliminated Lipid Nanoparticles for Systemic Delivery of RNAi Therapeutics 2013. https://doi.org/10.1038/mt.2013.124.

[112] Chen Y, Liu W, Sun T, Huang Y, Wang Y, Deb DK, et al. ,25-Dihydroxyvitamin D Promotes Negative Feedback Regulation of Toll-Like Receptor Signaling via Targeting MicroRNA-155-SOCS1 in Macrophages. J Immunol 2013;190:3687–95. https://doi.org/10.4049/jimmunol.1203273.

Appendix A- NTA Results of AntimiR-155 Transfection of AMSCs and Isolation of EVs

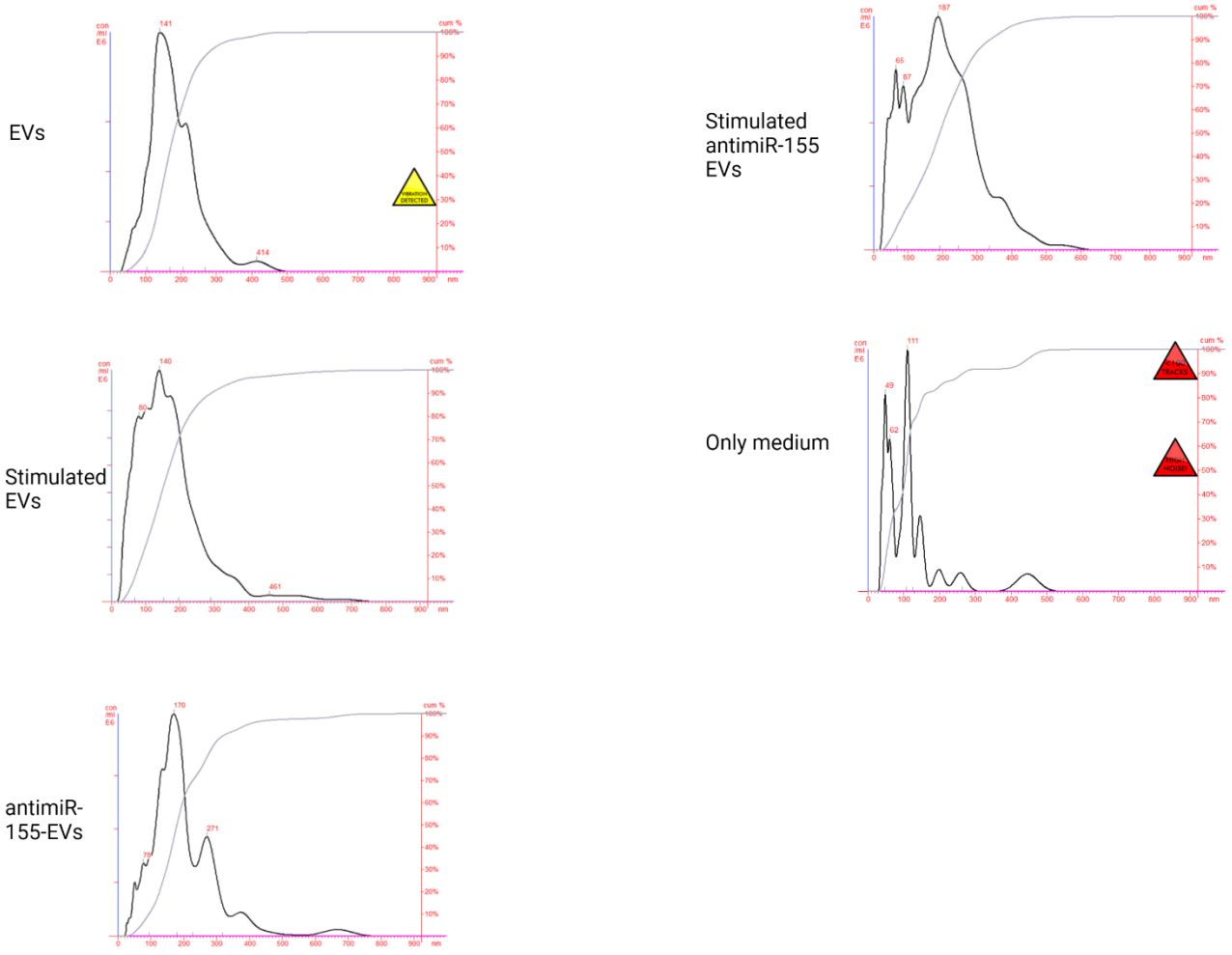

Figure 31: NTA analysis- Concentration graphics of AMSC derived EVs. Y axis of the graphic represent the concentration of the EVs, and the X axis represent the size distribution.

Appendix B- RNA Isolation with TRIzol™

1. Start with removing growth medium and adding TRIzol™. We used 300µl TRIzol™ for 250.000 cell seeding per well.
2. Pipet the lysate up and down several times to homogenize. (very important) and transfer your samples to Eppendorfs.
3. Incubate for 5 minutes to allow complete dissociation of the nucleoproteins complex and add 60µl chloroform.
4. Incubate for 2–3 minutes and centrifuge the sample for 15 minutes at 12,000 × g at 4°C.
5. Transfer the aqueous phase containing the RNA to a new tube by angling the tube at 45° and pipetting the solution out. Use 100µl pipet tip. If you pipet 150µl, it gives very high RNA concentration without transferring interphase. Throw away the pink part.
6. Add 150µl isopropanol on top of isolated RNA and Incubate for 10 minutes at 4°C (or on ice).
7. Centrifuge for 10 minutes at 12,000 × g at 4°C.
8. Discard the supernatant with a micropipette. Be very careful and slow, if you remove the supernatant very fast, most probably you will remove most of the RNA pellet as well because the pellet is not visible to eye.
9. Resuspend the pellet in 300µl of 75% ethanol. (The RNA can be stored in 75% ethanol for at least 1 year at –20°C, or at least 1 week at 4°C.)
10. Vortex the sample briefly, then centrifuge for 5 minutes at 7500 × g at 4°C.
11. Discard the supernatant with a micropipettor.
12. Air dry the RNA 10 min (lid open on ice under the hood)
13. Resuspend the pellet in 50 µL of RNase-free water
14. Incubate in a water bath or heat block set at 55–60°C for 10–15 minutes. (not always necessary)

Appendix C- cDNA Synthesis For Stem-loop PCR

Make your calculations according to the RNA isolation. 1000 ng of RNA was used for cDNA synthesis. RevertAid cDNA kit was used.

1. Into the small red tubes, first water, then RNA and lastly stem-loop primer (1µl) was added.
2. Samples put in a water bath 65 C for 5 min. (Water did not touch the cap)
3. Reaction mix was prepared according to the 13 sample. Components were added in ordered as below;

5X Reaction Buffer	4 µL
RiboLock RNase Inhibitor (20 U/µL)	1 µL
10 mM dNTP Mix	2 µL
RevertAid M-MuLV RT (200 U/µL)	1 µL

4. Reaction mix was added to the RNA samples (8µl).
5. Samples were put in Thermal cycler and the program was arranged to ;
   42°C for 60 min,
   70°C for 5 min,
   4°C for 60 min.
6. Samples were kept in the fridge (-20).

Amount of RNA (ng)*	1000						
Volume diluted RNA	11						
Volume iScript mix	9						
Total volume	20						
			For cDNA				
Sample	Name	Conc (ng/µl)	V RNA (µl)	V H20 (µl)	Stemloop primer	Reaction mix	[C] (ng/ul)
1	M0 Trizol	418.57	2.39	8.61	1.00	8.00	50
2	M1 Trizol	258.81	3.86	7.14	1.00	8.00	50
3	M2 Trizol	228.7	4.37	6.63	1.00	8.00	50
4	M0 kit	181.06	5.52	5.48	1.00	8.00	50
5	M1 kit	200.75	4.98	6.02	1.00	8.00	50
6	M2 kit	211.98	4.72	6.28	1.00	8.00	50
		for 1 sample	(for 12 samples)				
	Reaction buffer	4	52				
	Rnase inhibitor	1	13				
	dNTP mix	2	26				
	RevertMix	1	13				

Figure 32: Example calculations for cDNA synthesis.

Appendix D- AMSC Isolation from Mouse Epididymis Tissue

1. Add the adipose tissue into 5ml DMEM containing tube and incubate 15 min
2. Centrifuge 200g for 7 min at 4 C
3. Prepare 2% collagenase – 40 mg collagenase in 20 ml HBSS
4. Remove the tissue from the tube, wash with HBSS and put on the culture dish and mince it with scissors
5. Add 4ml digestion buffer in 13ml culture tube and add the minced tissue.
6. Incubate in thermaline shaker around 60 min.
7. After shaker, transfer the content to 50ml tubes and add 9 ml of DMEM with 10% FBS (add it first into 15ml tubes to take all the cells on the walls).
8. Mix gently 4 times
9. Get 70 uM cell strainer. Strain the content to another 50 ml tube by using 25 ml pippet. Add 1ml more DMEM to remove cells from the strainer.
10. Transfer the flow through to 15ml tube.
11. Centrifuge 600g 10 min at 4C
12. Remove supernatant.
13. Resuspend it with 5ml of PBS
14. Centrifuge 400g 10 min at 4C
15. Remove supernatant.
16. Add 5 ml of PBS. Take 10ul to the counting chamber. Calculate how much cell you have.
17. For T25 flask max medium should be 5 ml
18. And cell number should be around 2.5 x10^6
19. Centrifuge 400g 10 min at 4C
20. Remove supernatant
21. Add 5ml of DMEM containing 10% FBS and 1%P/S
22. Incubate overnight. The next day;
23. Prepare 10%FBS medium containing 5 ng/mL basic FGF (stock 100ug/ml B004, stock in the freezer is 50ng/ml)(Add 0.5ml of 50ng/ml FGF containing medium to 4.5 ml medium for T25. Add 1.5ml of 50ng/ml FGF containing medium to 13.5 ml medium for T75)
24. Adherent stem cells fraction therefore nonadherent cells will be removed, the medium will be changed into a fresh one with FGF-2. (Collect the first medium in another flask to not loose cells)

The third to fifth passages of ADSCs will be used for the experiments. (Every 2 days new medium)
Note: When you detached the cells, some of them are not easily detached and sticked to the surface. Those cells are not AMSCs. In addition, AMSC morphology is elongated, rounds cells are not MSCs.